bioRxiv preprint doi: https://doi.org/10.1101/744557; this version posted May 10, 2020. The copyright holder for this preprint (which was not certified by peer review) is the author/funder, who has granted bioRxiv a license to display the preprint in perpetuity. It is made available under aCC-BY-NC-ND 4.0 International license.

Title: The *Setaria viridis* genome and diversity panel enables discovery of a novel domestication gene

Authors: Sujan Mamidi[1,*], Adam Healey[1,*], Pu Huang[2,5,*]Jane Grimwood[1], Jerry Jenkins[1], Kerrie Barry[3], Avinash Sreedasyam[1], Shengqiang Shu[3], John T. Lovell[1], Maximilian Feldman[2,6], Jinxia Wu[1,7], Yunqing Yu[2], Cindy Chen[3], Jenifer Johnson[3], Hitoshi Sakakibara[4,8], Takatoshi Kiba[4,8], Tetsuya Sakurai[4,9], Rachel Tavares[2,10], Dmitri A. Nusinow[2], Ivan Baxter[2], Jeremy Schmutz[1,3], Thomas P. Brutnell[2,7], Elizabeth A. Kellogg[2,**]

[1] HudsonAlpha Institute for Biotechnology, Huntsville, Alabama, USA

[2] Donald Danforth Plant Science Center, 975 North Warson Road, St. Louis, MO 63132, USA

[3] Department of Energy Joint Genome Institute, Lawrence Berkeley National Laboratory, 1 Cyclotron Road, Berkeley, CA 94720, USA

[4] RIKEN Center for Sustainable Resource Science, Tsurumi, Yokohama 230-0045, Japan

[5] present address: BASF Corporation, 26 Davis Dr., Durham, NC 27709, USA

[6] present address: USDA-ARS Temperate Tree Fruit and Vegetable Research Unit, 24106 N. Bunn Rd., Prosser, WA 99350, USA

[7] Biotechnology Research Institute, Chinese Academy of Agricultural Sciences, Beijing 100081, China

bioRxiv preprint doi: https://doi.org/10.1101/744557; this version posted May 10, 2020. The copyright holder for this preprint (which was not certified by peer review) is the author/funder, who has granted bioRxiv a license to display the preprint in perpetuity. It is made available under aCC-BY-NC-ND 4.0 International license.

[8] present address: Graduate School of Bioagricultural Sciences, Nagoya University, Nagoya 464-8601, Japan

[9] present address: Multidisciplinary Science Cluster, Kochi University, Nankoku, Kochi, 783-8502, Japan

[10] present address: Biology Department, University of Massachusetts, Amherst, MA 01003 USA

* These authors contributed equally to this paper.

** Author for correspondence

bioRxiv preprint doi: https://doi.org/10.1101/744557; this version posted May 10, 2020. The copyright holder for this preprint (which was not certified by peer review) is the author/funder, who has granted bioRxiv a license to display the preprint in perpetuity. It is made available under aCC-BY-NC-ND 4.0 International license.

Abstract

Diverse wild and weedy crop relatives hold genetic variants underlying key evolutionary innovations of crops under domestication. Here, we provide genome resources and probe the genetic basis of domestication traits in green millet (*Setaria viridis*), a close wild relative of foxtail millet (*S. italica*). Specifically, we develop and exploit a platinum-quality genome assembly and *de novo* assemblies for 598 wild accessions to identify loci underlying a) response to climate, b) a key 'loss of shattering' trait that permits mechanical harvest, and c) leaf angle, a major predictor of yield in many grass crops. With CRISPR-Cas9 genome editing, we validated *Less Shattering1* (*SvLES1*) as a novel gene for seed shattering, which is rendered non-functional via a retrotransposon insertion in *SiLes1*, the domesticated loss-of-shattering allele of *S. italica*. Together these results and resources project *S. viridis* as a key model species for complex trait dissection and biotechnological improvement of panicoid crops.

bioRxiv preprint doi: https://doi.org/10.1101/744557; this version posted May 10, 2020. The copyright holder for this preprint (which was not certified by peer review) is the author/funder, who has granted bioRxiv a license to display the preprint in perpetuity. It is made available under aCC-BY-NC-ND 4.0 International license.

Introduction

Warm season C_4 grasses (subfamily Panicoideae) such as maize, sorghum and most species of millet are mainstays of industrial and small-holder agriculture, and include most major biofuel feedstocks. Crucially, C_4 photosynthesis is most productive under the hot and dry conditions that are predicted to become more prevalent over the coming decades[1-3]. While contemporary breeding of Panicoideae crops targets a trade-off between stress tolerance and yield, de novo domestication of wild Panicoideae species may provide an alternative path to develop novel bioproducts, fuels and food sources. However, the plants in the Panicoideae are known for long lifespans and large or complex genomes, creating the need for a practical experimental model that can be used for rapid discovery of gene structure and function and biotechnological improvement of related crops.

Setaria viridis (green foxtail) has emerged as such a model[4-6]. Plants are small (Figure 1a), diploid, have a short life cycle (seed to seed in 8-10 weeks), a small genome (ca. 500 Mb), and are self-compatible, with a single inflorescence that often produces hundreds of seeds. Transformation is efficient, and amenable to CRISPR-Cas9 mediated mutagenesis. These features have enabled use of *S. viridis* for studies of photosynthetic mechanisms[7-11], drought tolerance[12], cell wall composition[13-15], floral and inflorescence development[16,17], leaf anatomy[18], secondary metabolism[19], plant microbiomes[20,21], aluminum tolerance[22], defense responses[23], and even inspiration for engineering applications[24] (Figure S1).

As in most wild species, seeds of *S. viridis* fall off the plant at maturity, a process known as shattering[25]. While essential for dispersal in natural ecosystems, shattering is

bioRxiv preprint doi: https://doi.org/10.1101/744557; this version posted May 10, 2020. The copyright holder for this preprint (which was not certified by peer review) is the author/funder, who has granted bioRxiv a license to display the preprint in perpetuity. It is made available under aCC-BY-NC-ND 4.0 International license.

undesirable in cultivation and humans have selected for non-shattering mutants since the dawn of agriculture[26-28]. Such domesticates include *Setaria italica* (foxtail millet), the domesticated form of *S. viridis*, which is grown as a crop in Asia[29-31]. Improvement of some current crops (e.g. African fonio and North American wildrice) is hindered because shattering causes high losses at harvest[32-34]. Thus identification of genes

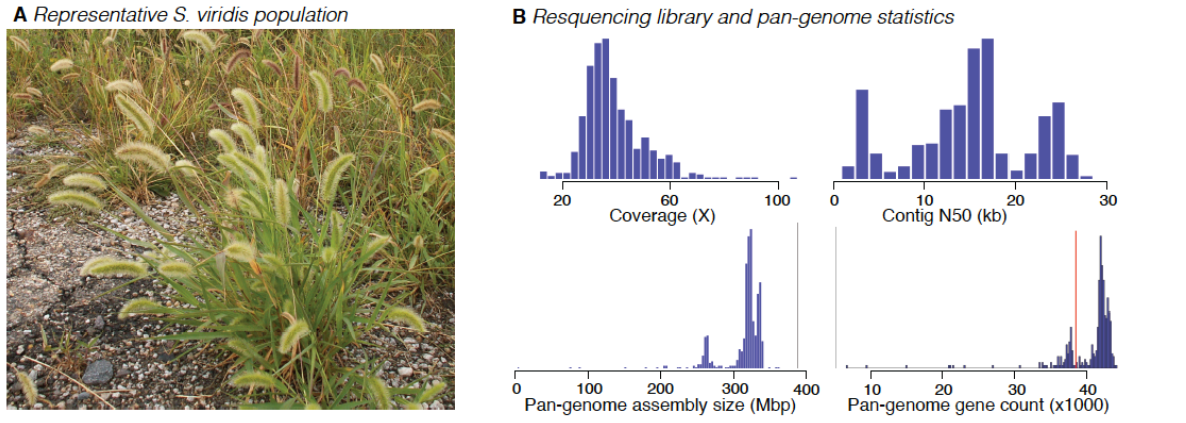

Fig. 1. a *Setaria viridis*, in its common highly disturbed habitat next to a road. **b** Average library coverage, contig N50 (Kb), pan-genome assembly size, and number of genes per library; red vertical line in lower right panel represents the number of genes necessary for a library to be included for PAV analysis (n=39,000).

critical for shattering has direct agronomic benefit.

Human selection on wild grasses could only have been effective if there is standing variation in genetic loci that affect shattering. However, to our knowledge no previous study has succeeded in cloning such loci via association studies of natural diversity. Most previous efforts have instead relied on crosses between domesticated plants and their wild progenitors, and genes and QTL identified in such studies are, for the most part, not conserved among species[25,35,36]. We infer that many shattering-related loci remain to be identified.

bioRxiv preprint doi: https://doi.org/10.1101/744557; this version posted May 10, 2020. The copyright holder for this preprint (which was not certified by peer review) is the author/funder, who has granted bioRxiv a license to display the preprint in perpetuity. It is made available under aCC-BY-NC-ND 4.0 International license.

In the work reported here, we surveyed natural populations of *S. viridis* and found allelic variation at a novel locus associated with seed shattering. We deployed a large sequence-based resource for *S. viridis*, analyzed its population structure using single-nucleotide polymorphisms (SNPs) and presence-absence variation (PAV) of individual genes, and tested for signatures of selection. Genome-wide association studies (GWAS) identified QTL for response to the abiotic environment and also a shattering-related locus, *Less shattering1* (*Les1*). Function of *Les1* was validated with genome editing. The orthologous gene in *S. italica* is disrupted by a transposon, indicating that the locus also contributed to domestication. In a parallel study, we identified a locus controlling leaf angle, a trait with clear agronomic implications. Data presented here show that genomics and biotechnological resources in *S. viridis* can be used to accelerate our mechanistic understanding of genetic processes and thereby contribute to enhanced and stabilized yield.

A complete genome and genomic model for the Panicoideae

We have developed significant new resources for the *Setaria* community. A new assembly was generated for the *S. viridis* reference line 'A10.1', using a combination of long-read Pacbio and Illumina sequencing technologies. The final version 2.0 release is a complete telomere-to-telomere chromosomal assembly, containing 395.1 Mb of sequence in 75 contigs with a contig N50 of 11.2 Mb and a total of 99.95% of assembled bases in nine chromosomes. This is a major improvement over previous *S. viridis* genome releases, which had a contig N50 of 1.6 MB, and ca. 94% of reads in contigs. The associated gene annotation is equally complete (BUSCO score [37] on

bioRxiv preprint doi: https://doi.org/10.1101/744557; this version posted May 10, 2020. The copyright holder for this preprint (which was not certified by peer review) is the author/funder, who has granted bioRxiv a license to display the preprint in perpetuity. It is made available under aCC-BY-NC-ND 4.0 International license.

106 Embryophyta for the gene set v2.1 is 99%) describing 38,334 gene models and 14,125
107 alternative transcripts.

108 To complement the genome assembly and probe the genetic architecture of
109 complex traits we conducted deep resequencing (mean of 56M high quality paired end
110 reads, 42.6X coverage) of 598 *S. viridis* diversity samples using Illumina 2x150 paired
111 end (PE) libraries (Figure 1b; metadata and sequence accession numbers in Table S1).
112 Each library was subsequently assembled into a pan-genome database. While less
113 contiguous than the long-read based A10.1 genome (mean n. contigs: 75,001; Contig
114 N50: 16.2 Kb), total assembled bases were very similar (mean assembled bases =
115 322.5 M) (Figure 1b).

116

117 **Multiple introductions from Eurasia underlie distinct North American gene pools**

118 The history of *S. viridis* in North America is unknown, although previous phylogenetic
119 studies place it within a clade of Asian genotypes [38,39]; indicating that Eurasia is the
120 native range while North America represents a recent and likely human-associated
121 range expansion. To understand the relationship of the North American samples to
122 samples from the Old World, we called 8.58M single nucleotide polymorphisms (SNPs)
123 among our 598 Illumina libraries (Table S1). We then extracted polymorphisms
124 comparable to the genotype-by-sequencing (GBS) data from previously-published
125 Illumina sequence data for 89 non-US samples collected in China, Canada, Europe and
126 Middle East [40]. We then tested for population structure using fastStructure [41] and
127 Admixture [42]. Overall, we find four distinct subpopulations, all of which are found both in
128 North American and Eurasia (Figure 2a, b). This pattern is expected if *S. viridis*

bioRxiv preprint doi: https://doi.org/10.1101/744557; this version posted May 10, 2020. The copyright holder for this preprint (which was not certified by peer review) is the author/funder, who has granted bioRxiv a license to display the preprint in perpetuity. It is made available under aCC-BY-NC-ND 4.0 International license.

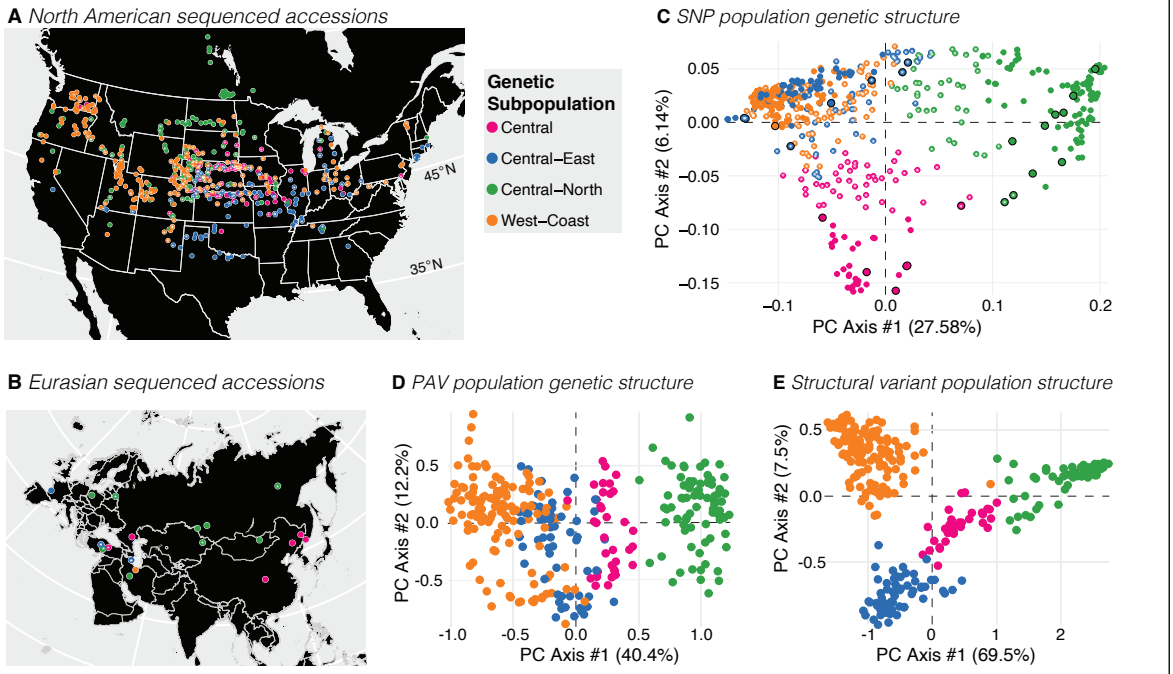

Fig. 2. PAV and SNP diversity of subpopulations. **a** Geographic distribution and population assignment of North American accessions based on SNP data. **b** Geographic distribution and population assignment of Eurasian accessions based on SNP data. **c** PCA of SNP data, showing placement of North American samples among Eurasian ones. **d** PCA of PAV variants, excluding admixed individuals. **e** PCA of structural variants, excluding admixed individuals. Both SNP and PAV data clearly separate the Central-North population (green) from the others, and the structural variants distinguish all populations. *, accession is admixed; black rim on circle, accession is in its native range.

diversified throughout Eurasia, was introduced to North America from several different sources, and then dispersed widely.

To define the evolutionary and biogeographical history of North American *S. viridis*, we conducted an identical population structure analysis with all SNPs in our resequencing panel. Of the 8.58 million SNPs (one SNP for every 21.6 bp), 430K mapped to exons (primary transcripts), 182K SNP were missense, 5K were nonsense, and 243K were silent. As with the GBS data, this analysis identified four main sub-populations (Central; Central-East; Central-North; West-coast; Figure S2). Not all individuals clustered uniquely into a single subpopulation; 382 genotypes were ‘pure’

bioRxiv preprint doi: https://doi.org/10.1101/744557; this version posted May 10, 2020. The copyright holder for this preprint (which was not certified by peer review) is the author/funder, who has granted bioRxiv a license to display the preprint in perpetuity. It is made available under aCC-BY-NC-ND 4.0 International license.

and assigned to a single subpopulation while 216 individuals were 'admixed' (Q < 0.7). These subpopulations trace their origins to distinct Eurasian gene pools: the 'Westcoast' subpopulation was closely related to samples from a genetic subpopulation that spanned the northern Middle East region; the closest relatives of the USA 'Central-North' subpopulation were found from northern Europe through Siberia; the Eurasian members 'Central-East' subpopulation were restricted to northern Iran and Afghanistan; and samples from China exclusively group with the 'Central' USA subpopulation (Figure 2b, c). The Central USA population, whose Eurasian relatives inhabit a range from China to Turkey, had the highest SNP diversity, highest number of private alleles, and lowest mean linkage disequilibrium (LD) of all the populations (Table S2). Such elevated diversity could be driven by larger or multiple founding populations.

Pan-Genome gene presence-absence variation mirrors SNP diversity

While SNPs serve as excellent proxies of total genetic diversity, previous work has demonstrated that larger-scale variation such as gene presence-absence and structural variants may underlie adaptation in nature and crop improvement[43-46]. To capture the set of all genes in all accessions of *S. viridis* (i.e., the pan-genome), we needed to identify genes that were missing or not annotated in the v2.1 gene set reference. Accordingly, we identified proteins in *Setaria italica* (v2.2), *Zea mays* (v.PH207) and *Sorghum bicolor* (v3.1) that were not shared with (i.e., not orthologous to) those in *S. viridis* (v2.1) and determined which were present in at least one member of the non-admixed diversity panel (382 accessions). This set of proteins was then added to the set from *S. viridis* (v2.1) to identify a pan-genome of 51,323 genes. Within

bioRxiv preprint doi: https://doi.org/10.1101/744557; this version posted May 10, 2020. The copyright holder for this preprint (which was not certified by peer review) is the author/funder, who has granted bioRxiv a license to display the preprint in perpetuity. It is made available under aCC-BY-NC-ND 4.0 International license.

this pan-genome, a core set of 39,950 genes occurred in 98% of all individuals. Of these core genes 32,732 were annotated in *S. viridis* (v2.1), with 3224, 3412, and 582 more identified based on similarity to *S. italica*, *Z. mays* and *S. bicolor* gene models, respectively. Discriminant function analysis of principal components (DAPC)[47,48], a multivariate method for identifying clusters of genes, identified an additional 5385 genes in 56% of all individuals (the "shell" set), and found the remaining 5987 in 12% of all individuals (the "cloud").

Consistent with other studies of pan-genome population genetics[49], the SNP- and PAV-based estimates of subpopulation structure are similar. Analysis of the "shell" gene PAV data revealed four subpopulations (n = 130, 78, 59, 35, respectively; Fig. 2d). Of the 203 non-admixed genotypes (that also had sufficient PAV data), 190 (94%) assigned to the same genetic subpopulation as in the SNP analysis. The Central-North population is clearly distinct in both PAV and SNP data (Fig. 2c), and when all structural variants are considered, the four populations are distinct (Fig. 2e). 4,062 genes are significantly over- or under-represented among subpopulations ($P < 0.05$; X^2- test, with Benjamini-Hochberg correction), with 45 private alleles (MAF > 0.1) specific to particular subpopulations (Table S3). KEGG and GO enrichment analyses for over-represented genes in each population found pathways relating to biosynthesis of secondary compounds, and genes involved in defense response to pathogens or herbivores Figure S3.

Our PAV data connect published QTL studies with population-level processes. For example, a study of drought response in *S. viridis* found a strong-effect QTL significant for plant size, water loss, and WUE across all tested environments [50].

bioRxiv preprint doi: https://doi.org/10.1101/744557; this version posted May 10, 2020. The copyright holder for this preprint (which was not certified by peer review) is the author/funder, who has granted bioRxiv a license to display the preprint in perpetuity. It is made available under aCC-BY-NC-ND 4.0 International license.

Investigation within the pan-genome found an *S-phase kinase associated protein1* (*Skp1)* homolog (Sevir.2G407800) within 50Kb of the associated SNP that was common in the Central-North population (present in 65% of individuals), while significantly under-represented in the Central-East (present in 5% of individuals) ($p < 4.3 \times 10^{-15}$). SKP1 proteins are part of the E3 ubiquitin ligase complex that leads to protein degradation[51]; while the physiological role of this particular SKP1 homolog is unknown, the fact that it falls within a known QTL interval and is differentially represented in two populations suggests it may be a candidate for future investigation.

Selection and correlation with climate in the new range of *S. viridis*

Combined, the PAV and SNP data clearly demonstrate massive genetic diversity and distinct gene pools to target molecular dissection of agriculturally important traits, including response to the environment. While we have shown that genetic variation in North American *S. viridis* reflects multiple introductions, we also observe pervasive genetic and biogeographic admixture. These factors, combined with its rapid cycling and weedy life history, indicate that adaptation to climate may underscore a biogeographic range expansion across much of the continent. To test this hypothesis, we characterized the environment for each accession using principal components analysis (PCA) of the Worldclim[52] environmental variables. To overcome collinearity among the climate variables (Figure S4), we transformed the 19 variables into the first three principal components (36.13%, 30.07% and 16.36% variance explained; factor loadings in Table S4), which served as response variables for three GWAS analyses. To control for population structure, we also supplied a set of three SNP-derived kinship PC axes which explain 15.34% of the genetic relatedness in our panel.

bioRxiv preprint doi: https://doi.org/10.1101/744557; this version posted May 10, 2020. The copyright holder for this preprint (which was not certified by peer review) is the author/funder, who has granted bioRxiv a license to display the preprint in perpetuity. It is made available under aCC-BY-NC-ND 4.0 International license.

While the first bioclimatic PC axis was not significantly associated with any SNP markers, PC2 had one association (Chr01: 37,770,697) (Figure S5) and PC3 identified several peaks with a total of 140 significant markers (Bonferroni corrected p-value, 5.82e-09). PC3 is loaded by climatic variables relating to extremes of precipitation and temperature. Of the 140 PC3 hits, 66 fall within 16 genes (Table S5). Genes within 100 Kbp of the significant markers were associated with organellar genome maintenance (GO:0033259, GO:0000002, GO:0006850), protein breakdown (GO:0045732), gibberellic acid homeostasis (GO:0010336), and fucose metabolism (GO:0006004, GO:0042353) (Table S6).

Despite the relatively small number of clear associations with parameters of the abiotic environment, both Tajima's D and iHS found multiple genes under selection in the four populations (Figure S6; Table S7). The two tests have different underlying assumptions and methods; genes that appear as outliers in both tests and annotations that arise repeatedly are excellent candidates for further investigation. For example, in most subpopulations we find selected genes consistently enriched in flavonoid (and other derivatives of phenylalanine) metabolism GO terms and KEGG pathways, processes that are often underlie responses to herbivores and pathogens and could be involved in local adaptation. However, selection on other processes and pathways appears to be specific to only one subpopulation. For example, genes involved in pH reduction in the Central-North population are identified by both tests, although interpretation of this result would require investigation of individual sets of genes and their tissue localization. Together, the bioclim GWAS and tests for selection show that *S. viridis* can provide testable hypotheses of gene function and phenotypic output.

bioRxiv preprint doi: https://doi.org/10.1101/744557; this version posted May 10, 2020. The copyright holder for this preprint (which was not certified by peer review) is the author/funder, who has granted bioRxiv a license to display the preprint in perpetuity. It is made available under aCC-BY-NC-ND 4.0 International license.

A novel gene, *SvLes1*, controls seed shattering in *S. viridis*

We deployed the new high quality genome, pan-genome and population genetic analyses to link genotypic diversity to the agronomically important phenotype of reduced shattering. We tested a subset of lines for seed shattering using a simple shattering index, in which mature panicles were scored for shattering on a scale of 1 (low) to 7 (high; Table S8). GWAS identified a single strong QTL (peak $-\log_{10} P > 30$) for seed shattering on chromosome 5 (Figure 3a) a region of approximately 2Mb above the experiment-wise p=0.01 Bonferroni correction threshold. In this region, 119 mutations, primarily missense, alter protein sequences relative to the reference; we used PROVEAN[53] to predict deleterious mutations that are more likely to alter the biological function of protein products. Combining this prediction and the association score of SNPs (Figure 3b), we prioritized a single G-T polymorphism (Chr_05:6849363) in a gene encoding a MYB transcription factor, *SvLes1* (Sevir.5G085400, similar to Sobic.003B087600 from *Sorghum bicolor* and ZM00001d040019_T001 from *Zea mays*), with two MYB DNA-binding domains. The mutation leads to a R84S substitution in the second MYB domain of *SvLes1* (Figure 3c). We name these two alleles *SvLes1-1* and *SvLes1-2*, associated with high seed shattering and reduced shattering, respectively. The *SvLes1-2* allele appears in 24% of the 215 accessions of the GWAS panel, and clearly associates with reduced shattering scores (p=6.53E1-33, 2-tailed test; Table S8). The reference line A10.1 is among these reduced-shattering lines.

To validate *SvLes1* as the causal gene, we used CRISPR-Cas9 to create additional alleles. We disrupted the wild type, high-shattering allele *SvLes1-1* in the accession ME034v (corresponding to accession TB0147) to create several novel, non-

bioRxiv preprint doi: https://doi.org/10.1101/744557; this version posted May 10, 2020. The copyright holder for this preprint (which was not certified by peer review) is the author/funder, who has granted bioRxiv a license to display the preprint in perpetuity. It is made available under aCC-BY-NC-ND 4.0 International license.

functional alleles. Sequence analysis of *SvLes1-CRISPR1* revealed an adenine insertion at position 149 of the transcript (Figure 3d), leading to a frameshift mutation predicted to completely abolish gene function thereby creating non-shattering plants. After segregating out the transgenes encoding Cas9 and guide RNAs, homozygotes of *SvLes1-CRISPR1* were phenotypically examined in the T3 generation.

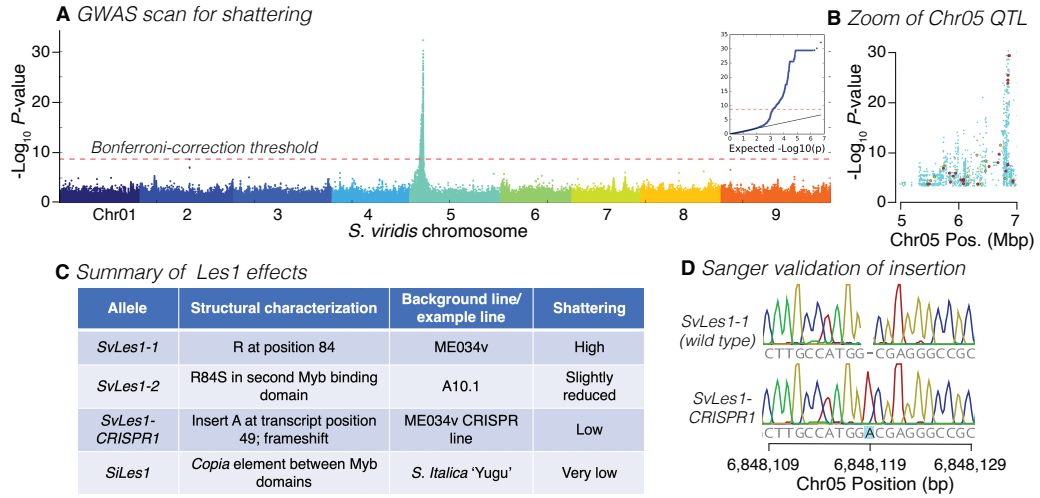

Allele	Structural characterization	Background line/ example line	Shattering
SvLes1-1	R at position 84	ME034v	High
SvLes1-2	R84S in second Myb binding domain	A10.1	Slightly reduced
SvLes1-CRISPR1	Insert A at transcript position 49; frameshift	ME034v CRISPR line	Low
SiLes1	*Copia* element between Myb domains	*S. Italica* 'Yugu'	Very low

Fig. 3. GWAS and cloning of *Les1*. **a** Manhattan plot of GWAS result, red line showing p=0.01 after Bonferroni correction. **b** Zoom in to peak on Chromosome 5; larger dots represent missense SNPs identified by snpEff. Different colors of missense SNPs indicate Provean score range (blue for >-2.5, green for <-2.5 and >-4.1, red for <-4.1; -2.5 and -4.1 represent 80% and 90% specificity). Lower scores indicate higher likelihood of deleterious effects of the mutation. **c** Table of *Les1* alleles in *S. viridis* (*Sv*) and *S. italica* (*Si*), with structural characteristics, background line, and shattering phenotype. **d** Sanger sequence validating the position of the adenine insertion (frameshift) in *SvLes1-CRISPR-1*.

To quantify seed shattering, we measured tensile strength of the abscission zone (AZ)[54,55]. We compared *SvLes1-CRISPR1* and *SvLes1-1*(both in an ME034v background) with *SvLes1-2* (in the A10.1, reduced shattering, background). *SvLes1-1* had the lowest tensile strength (high shattering), *SvLes1-2* tensile strength was slightly higher (less shattering), and *SvLes1-CRISPR1* had high tensile strength (reduced seed

bioRxiv preprint doi: https://doi.org/10.1101/744557; this version posted May 10, 2020. The copyright holder for this preprint (which was not certified by peer review) is the author/funder, who has granted bioRxiv a license to display the preprint in perpetuity. It is made available under aCC-BY-NC-ND 4.0 International license.

268 shattering) (Figure 4a,b). These results were confirmed with wind tunnel experiments
269 measuring the number of seeds released from the inflorescence and the distance they
270 traveled (Figure 4c). Few *SvLes1-CRISPR1* seeds were released from the plant,
271 whereas dozens of seeds were released from the *SvLes1-1* plants at six weeks after
272 heading. Seeds of the *SvLes1-CRISPR1* allele weighed significantly less than in

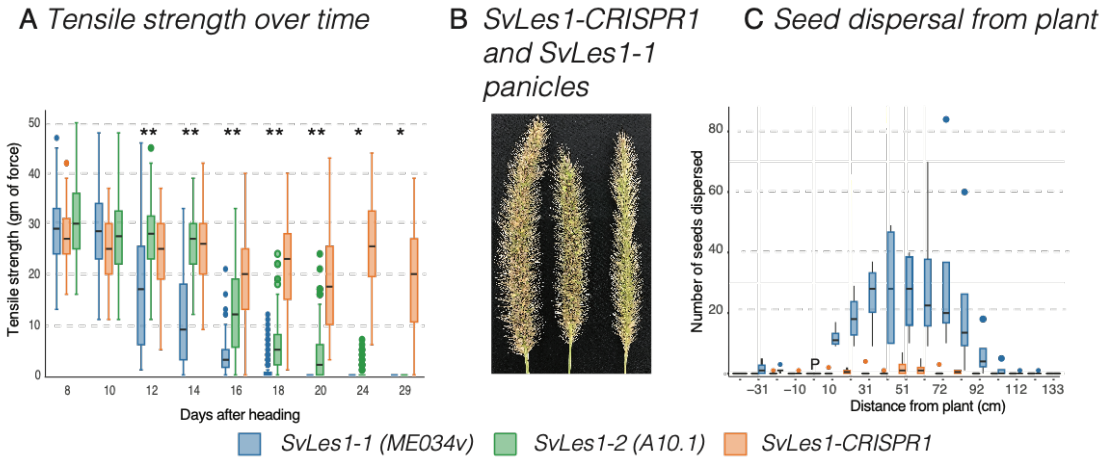

Fig. 4. Phenotypic characterization of *SvLes1-CRISPR1* mutants and naturally occurring alleles. **a** Force required to break the AZ (tensile strength in gm of force) in *SvLes1-1*, *SvLes1-2*, and *SvLes1-CRISPR1* lines, measured every two days starting at 8 days after heading. **b** Image of *S. viridis* high shattering (*SvLes1-1* in ME034), left two panicles) and *SvLes1-CRISPR1* mutant panicles seven weeks after heading. Both mutants have retained their seed, unlike ME034 which has shed most of its seed at this time point. **c** Seed dispersal distances in a wind tunnel, measured from four independent high shattering plants (*SvLes1-1* in ME034) and eight *SvLes1-CRISPR1* plants at week 6. Wind speed was 5 mph coming from the left of the diagram. The plant, indicated by P, was placed in middle of the tunnel; some seed fell on the windward side (negative distance values) due to oscillation of the plant. Although mean dispersal distance was approximately the same for both alleles, the *SvLes1-CRISPR1* plants released significantly fewer seeds at each distance that the *SvLes1-1* plants.

273

274 *SvLes1-1*, but germination percentage was unaffected (Figure S7). T3 offspring of T2
275 heterozygous plants segregated 3:1 shattering to non-shattering as expected for an

bioRxiv preprint doi: https://doi.org/10.1101/744557; this version posted May 10, 2020. The copyright holder for this preprint (which was not certified by peer review) is the author/funder, who has granted bioRxiv a license to display the preprint in perpetuity. It is made available under aCC-BY-NC-ND 4.0 International license.

276 induced mutation in a single gene, implying that the lines are isogenic except for the
277 mutant allele.

278 *SvLes1* is a transcription factor that has not been implicated in shattering in any
279 other species. Despite studies identifying shattering related genes in rice (e.g. *Sh4*[55],
280 *qSh1*[56], *Shat1*[57]) and sorghum (e.g. *Sh1*[58]), the cellular mechanism of shattering is not
281 known in any cereal, and recent data suggest that each species may be unique[36].
282 Unlike other grasses, the AZ in *Setaria viridis* is not histologically distinct and is only
283 subtly different from that in *S. italica*[25,54]. Cells and cell walls in the AZ are not clearly
284 different from their neighboring cells (demonstrated by multiple different cell wall stains
285 plus TEM[36]). Given this histology, we expected that the AZ of non-shattering mutants
286 would look like that of wild type plants, and indeed the anatomy and histology of
287 *SvLes1-CRISPR1* and *SvLes1-1*spikelets are indistinguishable (Figure S8).
288
289 **Recent transposable element insertion in *S. italica Les1* contributed to**
290 **domestication of foxtail millet**

291 Because *Setaria italica* (foxtail millet) is a domesticated (non-shattering)
292 derivative of *S. viridis*[29-31], we hypothesized that selection of non-shattering lines could
293 have identified rare alleles of *S. viridis* or *S. italica* early in the domestication process.
294 We discovered a ~6.5kb *copia* transposable element (*copia38*) inserted between the
295 two Myb domains of *SiLes1* in the *S. italica* line Yugu1. We call this the *SiLes1-TE*
296 (transposable element) allele. The disruption of the Myb domain strongly suggests
297 *SiLes1-TE* is a loss of function allele similar to *SvLes1-CRISPR1* and should also
298 produce a low shattering phenotype, thus potentially contributing to the domestication of

bioRxiv preprint doi: https://doi.org/10.1101/744557; this version posted May 10, 2020. The copyright holder for this preprint (which was not certified by peer review) is the author/funder, who has granted bioRxiv a license to display the preprint in perpetuity. It is made available under aCC-BY-NC-ND 4.0 International license.

299 foxtail millet. The *copia38* transposable element was aligned to each of the 598 *S.*
300 *viridis* re-sequenced lines to investigate whether any had the TE insertion in *SvLes1*.
301 Only two samples aligned to the *copia38* TE within the CDS sequence of *SvLes1*, but
302 the nucleotide identity and coverage of the alignments were poor (32% and 6%
303 respectively). In contrast, *Copia38* is nearly fixed among the foxtail millet lines
304 examined (78 out of 79).

305 Genome-wide, *S. italica* has about 22% of the SNP variation of *S. viridis* (based
306 on sequences generated in [59]), as expected given its domestication history. In the
307 *SiLes1* region, however, this number is significantly reduced to 4.1-8.2% of the diversity
308 in *S. viridis* depending on the size of the region compared (10-100 Kbp, Table S9)
309 ($p=0.0066$ based on 100,000 coalescent simulations of the ratio of π *italica*/π *viridis*).
310 These data hint that the low-shattering QTL might co-localize with a selective sweep.
311 Diversity is relatively high within the *S. italica* gene itself, which may mean that selection
312 is on a regulatory region or additional locus under the QTL or that the transposon
313 insertion has rendered *SiLes1* a pseudogene. Estimates of linkage disequilibrium (LD)
314 support this interpretation (Table S10). In *S. viridis* estimates of LD do not vary much
315 across intervals from 10 to 100 Kbp surrounding *SvLes1*. In *S. italica* on the other hand,
316 LD is nearly complete for the 20 kb region surrounding *SiLes1*. When that region is
317 expanded to 40 Kbp LD drops to levels approximating that in *S. viridis*. Taken together,
318 these data indicate either a selective sweep or purifying selection on a genomic region
319 that includes *SiLes1* and *copia38* in LD.

320 *SiLes1* has not been identified in other studies of *S. italica* and thus its potential
321 role in domestication is newly described here. Two strong QTL for shattering were

bioRxiv preprint doi: https://doi.org/10.1101/744557; this version posted May 10, 2020. The copyright holder for this preprint (which was not certified by peer review) is the author/funder, who has granted bioRxiv a license to display the preprint in perpetuity. It is made available under aCC-BY-NC-ND 4.0 International license.

identified in recombinant inbred lines derived from an *S. italica* x *S. viridis* cross (accessions B100 and A10.1, respectively)[60], but neither QTL encompasses *SiLes1*. Analysis of 916 diverse accessions of *S. italica* identified 36 selective sweeps, but the *SiLes1* region does not colocalize with any of them[59]. In addition, a previous study[54] found that tensile strength in two elite *S. italica* lines, Yugu1 and B100, is higher than that of the *SvLes1-CRISPR1* homozygotes reported here. Thus all previous data indicate that *SiLes1-TE* is but one of several loci contributing to the lack of shattering in foxtail millet.

Copia38 is a long terminal repeat (LTR) retroelement with two 451 bp LTR sequences. The LTRs for *Copia38* are identical across the entire pan-genome, suggesting that the insertion is recent, because mutations start to accumulate in the once-identical LTRs immediately after insertion of a TE. Phylogenetic analysis showed *Copia38* tightly clusters with a few homologous copies on a long branch, indicating a shared burst event for copies in this cluster (Figure S9). Pairwise distance among the copies suggests this burst was recent, on average about 45k (range 23k – 81k) years ago, assuming a neutral mutation rate of 6.5×10^{-9}/bp/year[61]. The copies from this burst only occur in Yugu1 but not in A10.1, suggesting a recent expansion just prior to domestication of *S. italica* that began approximately 8000 years ago[29-31].

Combining the results and evidence above, a plausible scenario is that the *SiLes1-TE* allele was a low frequency allele that was selected during domestication due to its favored low shattering phenotype, and spread quickly through the early foxtail millet land races. Later, the low shattering phenotype was further strengthened by additional loci with stronger effects (i.e. *SvSh1*[59,60]) during recent crop improvement.

bioRxiv preprint doi: https://doi.org/10.1101/744557; this version posted May 10, 2020. The copyright holder for this preprint (which was not certified by peer review) is the author/funder, who has granted bioRxiv a license to display the preprint in perpetuity. It is made available under aCC-BY-NC-ND 4.0 International license.

Genome editing technology today allows us to recreate a low-shattering phenotype from ancestral *S. viridis* alleles, mimicking the initial phase of foxtail millet domestication through a different novel allele *SvLes1-CRISPR1.*

Parallel genetic control of leaf angle in *S. viridis* and maize by *liguleless2* orthologs

The diversity panel is also a powerful tool for uncovering the basis of rare traits, including those of agronomic value. We discovered a single accession in the panel (TB0159) with reduced auricle development and markedly upright leaves (small leaf angle) (Figure 5a,b), a trait of considerable interest in the major crops maize and rice, where it has led to increased planting densities and higher yields[62-64]. As GWAS is not suitable for mapping traits with low frequency and strong effects, bulked segregant analysis (BSA)[17,40] was used to identify the associated genomic region. BSA is a process in which plants with and without a particular phenotype are pooled (bulked) and then each pool is sequenced. Regions or loci that differ between the two pools are then inferred to contain the mutations underlying the phenotype. TB0159 was crossed to A10.1, and the F1 plants showed wild type leaf angle, showing that small leaf angle is recessive. The wild type and small leaf angle trait in the F_2 population segregated at 264:153 which differs significantly from a 3:1 ratio (p=0.000238). This could be explained by partial dominance at a single locus, or by several loci controlling the phenotype. We proceeded assuming a single partially dominant causal gene for small leaf angle.

bioRxiv preprint doi: https://doi.org/10.1101/744557; this version posted May 10, 2020. The copyright holder for this preprint (which was not certified by peer review) is the author/funder, who has granted bioRxiv a license to display the preprint in perpetuity. It is made available under aCC-BY-NC-ND 4.0 International license.

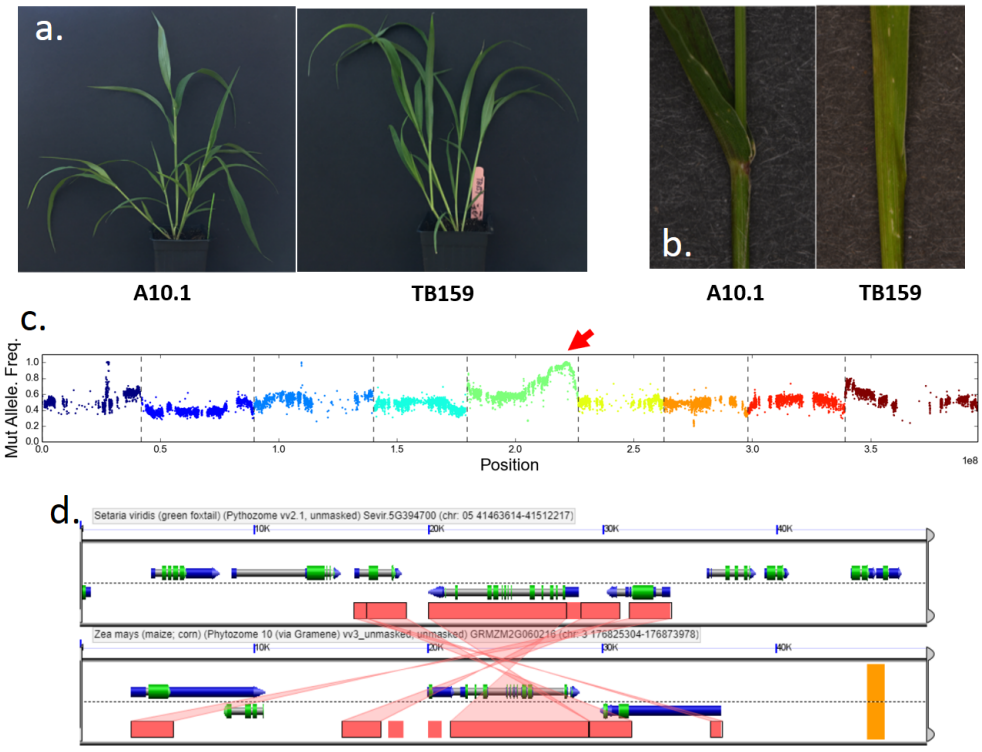

Fig. 5. Phenotype and mapping of small leaf angle. **a, b** Small leaf angle phenotype in TB159. **c** BSA mapping result, red arrow indicating QTL. **d** Synteny analysis around *SvLg2* and maize *lg2* locus.

With BSA, we coarsely mapped the reduced leaf angle phenotype to a homozygous region of ~800 kb on chromosome 5 (Figure 5c) that contained 104 disruptive SNPs and 687 indels (393 single bp). This region includes *SvLiguless2* (*SvLg2*) (Sevir.5G394700), the syntenic ortholog of *liguless2* in maize (Figure 5d), which is a transcriptional regulator that controls auricle development and leaf angle[65]. Because the small leaf angle phenotype is partially dominant and unique to TB0159 in the panel, the causal allele should be homozygous and occur only in that accession. We identified a homozygous G insertion (Chr_5:41489494) in the coding region of *SvLg2* of that is predicted to cause a frameshift. Accordingly, we hypothesize that this indel mutation might be the causal mutation for the small leaf angle in TB0159. As the ligule is a trait

bioRxiv preprint doi: https://doi.org/10.1101/744557; this version posted May 10, 2020. The copyright holder for this preprint (which was not certified by peer review) is the author/funder, who has granted bioRxiv a license to display the preprint in perpetuity. It is made available under aCC-BY-NC-ND 4.0 International license.

379 unique to grasses and has been a target for breeding programs, *S. viridis* can now be
380 used as a model system to rapidly dissect the molecular genetic network of Lg2, which
381 remains poorly resolved in maize and rice, to identify additional candidates for breeding
382 or engineering of this important architectural trait.

383 In summary, data presented here demonstrate the power of the *S. viridis* genome
384 and associated diversity lines for gene discovery. Together these tools permit discovery
385 of novel environmental associations and genes such as *SvLes1*, and additional insight
386 into genes such as *SvLg2* that have been identified from related systems. We show that
387 *S. viridis* resources can uncover the genetic basis of a trait when the genes are
388 unknown and likely differ from those in other related species. We also show that *S.*
389 *viridis* can be a model for investigating genes in which an orthologue is known in a crop.
390 Specifically, we have used the *S. viridis* genome and diversity panel to study the genetic
391 basis of seed shattering and leaf angle (*SvLes1* and *SvLg2*, respectively), traits that
392 influence crop yield by affecting harvestability, productivity and density of planting.
393

394 **Methods**

395

396 **Plant materials**

397 The reference line A10.1 is a descendant of the line used by Wang et al.[66] in early
398 RFLP maps. The original line was found to be heterozygous and thus A10.1 was
399 propagated via single-seed descent by Andrew Doust (Oklahoma State University,
400 Stillwater, OK, pers. comm.). It is thought to have originated in Canada. The other
401 reference, ME034 (also known as ME034v), was collected by Matt Estep (Appalachian

bioRxiv preprint doi: https://doi.org/10.1101/744557; this version posted May 10, 2020. The copyright holder for this preprint (which was not certified by peer review) is the author/funder, who has granted bioRxiv a license to display the preprint in perpetuity. It is made available under aCC-BY-NC-ND 4.0 International license.

State University, Boone, NC) in southern Canada as part of a diversity panel[39] included among the diversity lines sequenced here. Transformation is more efficient for ME034 than for A10.1 (Joyce van Eck, Boyce Thompson Institute, Ithaca, NY, pers. comm.) and thus the former is being used widely for functional genetic studies.

The 598 individuals of the diversity panel were collected over a period of several years. About 200 lines have been described in previous studies[39,67] whereas others were new collections added for this project. Individuals were propagated by single seed descent, although the number of generations varies by accession. *Setaria viridis* is inbreeding by nature (ca. 1%[67]), so we assume that initial heterozygosity was generally low and then further reduced in propagation.

Library creation and sequencing

To prepare DNA for sequencing of the reference line, 100 ng of DNA was sheared to 500 bp using the Covaris LE220 (Covaris) and size selected using SPRI beads (Beckman Coulter). The fragments were treated with end-repair, A-tailing, and ligation of Illumina compatible adapters (IDT, Inc) using the KAPA-Illumina library creation kit (KAPA biosystems). The prepared library was then quantified using KAPA Biosystem's next-generation sequencing library qPCR kit and run on a Roche LightCycler 480 real-time PCR instrument. The quantified library was then multiplexed with other libraries, and the pool of libraries was prepared for sequencing on the Illumina HiSeq sequencing platform using a TruSeq paired-end cluster kit, v3, and Illumina's cBot instrument to generate a clustered flowcell for sequencing. Sequencing

bioRxiv preprint doi: https://doi.org/10.1101/744557; this version posted May 10, 2020. The copyright holder for this preprint (which was not certified by peer review) is the author/funder, who has granted bioRxiv a license to display the preprint in perpetuity. It is made available under aCC-BY-NC-ND 4.0 International license.

of the flowcell was performed on the Illumina HiSeq2000 sequencer using a TruSeq SBS sequencing kit, v3, following a 2x150 indexed run recipe.

Plate-based DNA library preparation for Illumina sequencing was performed on the PerkinElmer Sciclone NGS robotic liquid handling system using Kapa Biosystems library preparation kit. 200 ng of sample DNA was sheared to 600 bp using a Covaris LE220 focused-ultrasonicator. Sheared DNA fragments were size selected by double-SPRI and then the selected fragments were end-repaired, A-tailed, and ligated with Illumina compatible sequencing adaptors from IDT containing a unique molecular index barcode for each sample library.

The prepared library was quantified using Kapa Biosystem's next-generation sequencing library qPCR kit and run on a Roche LightCycler 480 real-time PCR instrument. The quantified library was then multiplexed with other libraries, and the pool of libraries was then prepared for sequencing on the Illumina HiSeq sequencing platform using a TruSeq paired-end cluster kit, v3 or v4, and Illumina's cBot instrument to generate a clustered flowcell for sequencing. Sequencing of the flowcell was performed on the Illumina HiSeq2000 or HiSeq2500 sequencer using HiSeq TruSeq SBS sequencing kits, v3 or v4, following a 2x150 indexed run recipe.

Sequencing of the reference genome

We sequenced *S. viridis* A10.1 using a whole genome shotgun sequencing strategy and standard sequencing protocols. Sequencing reads were collected using Illumina HISeq and PACBIO SEQUEL platforms at the Department of Energy (DOE) Joint Genome Institute (JGI) in Walnut Creek, California and the HudsonAlpha Institute in Huntsville,

bioRxiv preprint doi: https://doi.org/10.1101/744557; this version posted May 10, 2020. The copyright holder for this preprint (which was not certified by peer review) is the author/funder, who has granted bioRxiv a license to display the preprint in perpetuity. It is made available under aCC-BY-NC-ND 4.0 International license.

Alabama. One 800 bp insert 2x250 Illumina fragment library (240x) was sequenced, giving 425,635,116 reads (Table S11). Illumina reads were screened for mitochondria, chloroplast, and PhiX contamination. Reads composed of >95% simple sequence were removed. Illumina reads <75bp after trimming for adapter and quality (q<20) were removed. For the PACBIO sequencing, a total of 36 P5C2 chips (4 hour movie time) and 41 P6C4 chips (10 hour movie time) were sequenced with a p-read yield of 59.09 Gb, with a total coverage of 118.18x (Tables S11, S12).

Genome assembly and construction of pseudomolecule chromosomes

An improved version 2.0 assembly was generated by assembling 4,768,857 PACBIO reads (118.18x sequence coverage) with the MECAT assembler[68] and subsequently polished using QUIVER[69]. The 425,635,116 Illumina sequence reads (240x sequence coverage) were used for correcting homozygous snp/indel errors in the consensus. This produced 110 scaffolds (110 contigs), with a contig N50 of 16.8 Mb, and a total genome size of 397.9 Mb (Table S13). A set of 36,061 syntenic markers derived from the version 2.2 *Setaria italica* release was aligned to the MECAT assembly. Misjoins were characterized as a discontinuity in the *italica* linkage group. A total of 15 breaks were identified and made. The *viridis* scaffolds were then oriented, ordered, and joined together into 9 chromosomes using syntenic markers. A total of 61 joins were made during this process. Each chromosome join is padded with 10,000 Ns. Significant telomeric sequence was identified using the TTTAGGG repeat, and care was taken to make sure that it was properly oriented in the production assembly.

bioRxiv preprint doi: https://doi.org/10.1101/744557; this version posted May 10, 2020. The copyright holder for this preprint (which was not certified by peer review) is the author/funder, who has granted bioRxiv a license to display the preprint in perpetuity. It is made available under aCC-BY-NC-ND 4.0 International license.

Scaffolds that were not anchored in a chromosome were classified into bins depending on sequence content. Contamination was identified using blastn against the NCBI nucleotide collection (NR/NT) and blastx using a set of known microbial proteins. Additional scaffolds were classified as repetitive (>95% masked with 24mers that occur more than 4 times in the genome) (26 scaffolds, 1.2 Mb), alternative haplotypes (unanchored sequence with >95% identity and >95% coverage within a chromosome) (15 scaffolds, 1.0 Mb), chloroplast (3 scaffolds, 164.5 Kb), mitochondria (5 scaffolds, 344.9 Kb), and low quality (>50% unpolished bases post polishing, 1 scaffold, 19.3 Kb). Resulting final statistics are shown in Table S14.

Finally, homozygous SNPs and INDELs were corrected in the release consensus sequence using ~60x of Illumina reads (2x250, 800 bp insert) by aligning the reads using bwa mem [70] and identifying homozygous SNPs and INDELs with the GATK's UnifiedGenotyper tool [71]. A total of 96 homozygous SNPs and 4,606 homozygous INDELs were corrected in the release. The final version 2.0 release contains 395.1 Mb of sequence, consisting of 75 contigs with a contig N50 of 11.2 Mb and a total of 99.95% of assembled bases in chromosomes (Table S14).

Completeness of the v2.0 assembly is very high. To further assess completeness of the euchromatic portion of the version 2.0 assembly, a set of 40,603 annotated genes from the *S. italica* release was used for comparison. The aim of this analysis is to obtain a measure of completeness of the assembly, rather than a comprehensive examination of gene space. The transcripts were aligned to the assembly using BLAT [72] and alignments ≥90% base pair identity and ≥85% coverage were retained. The screened alignments indicate that 39,441 (97.14%) of the *italica* genes aligned to the

bioRxiv preprint doi: https://doi.org/10.1101/744557; this version posted May 10, 2020. The copyright holder for this preprint (which was not certified by peer review) is the author/funder, who has granted bioRxiv a license to display the preprint in perpetuity. It is made available under aCC-BY-NC-ND 4.0 International license.

492 version 2.1 release. Of the unaligned 1,162 transcripts, 928 (2.28%) indicated a partial
493 alignment, and 234 (0.58%) were not found in the version 2.1 release.
494 To assess the accuracy of the assembly, a set of 335 contiguous Illumina clones
495 >20 Kb was selected. A range of variants was detected in the comparison of the clones
496 and the assembly. In 239 of the clones, the alignments were of high quality (< 0.01%
497 bp error) with an example being given in Figure S10a (all dot plots were generated
498 using Gepard [73]). The remaining 96 clones indicate a higher error rate due mainly to
499 their placement in more repetitive regions (Figure S10b). The major component of the
500 error in the 96 repetitive clones was copy number variation, which affected 50 of the
501 clones. These 50 clones accounted for >97% of all of the errors in the 335-clone set.
502 Excluding the clones with copy number variation, the overall bp error rate in the 285
503 clone set is 0.0098% (1,043 discrepant bp out of 10,601,785).
504
505 **Annotation**
506 Various Illumina RNA-seq reads were used to construct transcript assemblies using a
507 genome-guided assembler, PERTRAN[74]: 1B pairs of geneAtlas, 0.9B pairs of LDHH,
508 0.9B pairs of LLHC, and 176M other pairs. 109,119 transcript assemblies were
509 constructed using PASA[75] from RNA-seq transcript assemblies above.
510 Gene models of v1.1 on assembly v1.0 were lifted over to assembly v2.0 and
511 improved. The in-house gene model improvement (GMI) pipeline is as follows:
512 The genomic sequence of a locus is obtained, including introns if any and up to
513 1Kbp extensions on both ends unless they run into another gene. For intergenic space
514 less than 2Kbp, half of the intergenic distance is the extension for 2 adjacent loci. These

bioRxiv preprint doi: https://doi.org/10.1101/744557; this version posted May 10, 2020. The copyright holder for this preprint (which was not certified by peer review) is the author/funder, who has granted bioRxiv a license to display the preprint in perpetuity. It is made available under aCC-BY-NC-ND 4.0 International license.

515 locus sequences are mapped to a new genome using BLAT. Duplicate mappings are
516 resolved using the gene model's neighbors in original genome space. When a locus
517 genomic sequence is mapped to the new genome uniquely and 100%, the gene model
518 is perfectly transferred to the new genome. For the remaining gene models, both their
519 transcript and CDS sequences are mapped with BLAT to the region in the new genome
520 located by locus genomic sequence mapping above. Gene models are made from CDS
521 alignments with quality of 95% identity, 90% coverage and valid splice sites if any, and
522 are transferred if the resulting peptide is 70% or more similar to the original gene model
523 peptide. UTRs are added if any using transcript alignments. Remaining gene models
524 are mapped to the new genome using GMAP. Gene models based on GMAP
525 alignments with quality of 95% identity, 70% coverage and valid splice sites if any are
526 transferred if and only if the resulting gene model peptide is 70% or more similar to the
527 original gene model peptides and in the new genome location not occupied by
528 transferred gene models in earlier steps.

529 Non-overlapping complete ORFs from each PASA transcript assembly (TA) were
530 predicted if the ORF had good homology support or was long enough (300bp if multi
531 exons or 500bp if single exon). Proteins from *Arabidopsis thaliana*, rice, sorghum,
532 *Brachypodium distachyon*, *Setaria italica*, grape, soybean and Swiss-Prot eukaryote
533 were used to score TA ORFs using BLASTP. The TA ORFs were then fed into the
534 PASA pipeline where EST assemblies were obtained for gene model improvement
535 including adding UTRs. PASA improved gene model transcripts were compared to v1.1
536 lifted over models on how well the transcript CDS was supported by ESTs and/or
537 homologous protein, and not overlapped with repeats generated with RepeatMasker[76]

bioRxiv preprint doi: https://doi.org/10.1101/744557; this version posted May 10, 2020. The copyright holder for this preprint (which was not certified by peer review) is the author/funder, who has granted bioRxiv a license to display the preprint in perpetuity. It is made available under aCC-BY-NC-ND 4.0 International license.

538 for more than 20 percent. If PASA gene models of TA ORFs were better than lifted over
539 ones, the PASA gene models took over the lifted over ones. Otherwise, the lifted over
540 gene model stayed. The final gene model proteins were assigned PFAM, PANTHER
541 and gene models were further filtered for those with 30% or more of proteins assigned
542 to transposable element domains.

543 Locus model name was assigned by mapping forward v1.1 locus model if
544 possible using our locus name map pipeline; otherwise, a new name was given using
545 JGI locus naming convention that was used in v1.1 locus model naming. Our locus
546 name map pipeline is as following: a locus is said to be mapped and name mapped
547 forward if 1) the prior version and current version loci overlap uniquely and appear on
548 the same strand, and 2) at least one pair of translated transcripts from the old and new
549 loci are MBH's (mutual best hits) with at least 70% normalized identity in a BLASTP
550 alignment (normalized identity defined as the number of identical residues divided by
551 the longer sequence). For a given pair of prior version and current version transcripts at
552 mapped loci, transcript model names are mapped forward if either a) an MBH
553 relationship exists between the two proteins with at least 90% normalized identity or, b)
554 the proteins have at least 90% normalized identity and are not MBH, but the
555 corresponding transcripts sequences are (also with 90% normalized identity). This latter
556 rule is specifically to handle cases where the prior version and current version models
557 differ mainly by the addition of, or extension, of the UTR to a prior version model. These
558 rules allowed the model names of approximately 92% v1.1 gene models mapped
559 forward to v2.1.
560

bioRxiv preprint doi: https://doi.org/10.1101/744557; this version posted May 10, 2020. The copyright holder for this preprint (which was not certified by peer review) is the author/funder, who has granted bioRxiv a license to display the preprint in perpetuity. It is made available under aCC-BY-NC-ND 4.0 International license.

561 **Sequencing and assembly of the diversity panel**

562 After excluding seven lines because of low sequence coverage, 598 diversity samples
563 (metadata, including Sequence Read Archive (SRA) numbers in Table S1) were used
564 for diversity analysis. The samples were sequenced using Illumina paired end
565 sequencing (2*151bp) at the Department of Energy Joint Genome Institute (JGI, Walnut
566 Creek, CA, USA) and the HudsonAlpha Institute for Biotechnology (Huntsville AL, USA)
567 using Hiseq 2500 and NovoSeq6000. Individual de novo assemblies for each line were
568 constructed using Meraculous (v2.2.5)[77] with a kmer size of 51, selected to maximize
569 the contig N50 in the resultant assemblies, and to ensure that alternative haplotypes
570 would have the best chance of being split apart. To construct chromosomes for each
571 library, exons from the *S. viridis* gene set reference (v2.1; number of genes = 38,334;
572 number of exons = 289,357) were aligned to each Meraculous assembly (blastn,
573 word_size = 32), and exon alignments with identity >=90% and coverage >=85% were
574 retained. Scaffolds were joined into gene-based scaffolds based on exon alignments;
575 synteny and exon alignments were then used to order and orient the sequences into
576 chromosomes (Figure S11).
577
578 **SNP calling**
579 Reads from the diversity samples were mapped to *S. viridis* v2.1 using bwa-mem[78]. The
580 bam was filtered for duplicates using picard (http://broadinstitute.github.io/picard), and
581 realigned around indels using GATK[71]. Multi sample SNP calling was done using
582 SAMtools mpileup[79] and Varscan V2.4.0[80] with a minimum coverage of eight and a
583 minimum alternate allele frequency of four. An allele is confirmed to be homozygous or

bioRxiv preprint doi: https://doi.org/10.1101/744557; this version posted May 10, 2020. The copyright holder for this preprint (which was not certified by peer review) is the author/funder, who has granted bioRxiv a license to display the preprint in perpetuity. It is made available under aCC-BY-NC-ND 4.0 International license.

584 heterozygous using a binomial test for significance at a p-value of 0.05. Repeat content
585 of the genome was masked using 24bp kmers. Kmers that occur at a high frequency, up
586 to 5%, were masked. SNP around 25bp of the mask were removed for further analysis.
587 A SNP was included for further analysis if it had a coverage in 90% of the samples, and
588 a MAF > 0.01. Imputation and phasing were done in Beagle V4.0[81]. SNP Annotation
589 was performed using snpEff[82].
590
591 **Pan-genome and PAV analysis**
592 To assess presence/absence variation (PAV) of genes across the diversity panel,
593 admixed individuals were removed from the analysis, leaving 382 individuals (Q>=0.7).
594 We expected that some genes present in wild accessions of *S. viridis* (i.e. the pan-
595 genome) would be either missing or not annotated in the v2.1 reference gene set. To
596 capture these, we included not only proteins from *S. viridis* (v2.1 gene set) but also non-
597 orthologous proteins from *Setaria italica* (v2.2), *Z. mays* (v.PH207) and *S.bicolor*
598 (v3.1)(based on InParanoid comparisons[83]) and aligned these to chromosome
599 integrated assemblies from each of the four subpopulations using blat (-noHead -
600 extendThroughN -q=prot -t=dnax).
601 Genes from *S. viridis* and *S. italica* were considered present if they aligned with
602 greater than 85% coverage and identity, or at least 90% coverage and identity if the
603 exons were broken up and located on no more than three contigs. *Sorghum bicolor* and
604 *Zea mays* genes were considered present if they aligned with greater than 70% identity
605 and 75% coverage (to allow for greater divergence among sequences), or at least 80%
606 identify and coverage if the exons were broken up and located on no more than three

bioRxiv preprint doi: https://doi.org/10.1101/744557; this version posted May 10, 2020. The copyright holder for this preprint (which was not certified by peer review) is the author/funder, who has granted bioRxiv a license to display the preprint in perpetuity. It is made available under aCC-BY-NC-ND 4.0 International license.

607 contigs. Libraries with fewer than 39,000 genes considered present were excluded as
608 genes were likely lost due to low coverage/poor assembly, with 302 individuals
609 remaining for analysis. 67,079 genes were aligned to each assembly. After removing
610 genes that aligned poorly or not at all to any assembly, a total of 51,323 genes was
611 retained. The resultant PAV matrix (Table S15) was used to determine and cluster
612 genes into their pan-genome designation (core, shell, cloud)[74-76], using discriminant
613 function analysis of principal components (DAPC)[41]. Using successive Kmeans
614 clustering, three distinct clusters (based on BIC criteria) were discovered based on their
615 PAV observance across non-admixed individuals, designated core, shell and cloud.
616 Genomic coordinates for non-orthologous proteins in the pan-genome were determined
617 using the GENESPACE pipeline[74].

618 To discover which genes were over or under represented within each
619 subpopulation based on their expected observance, a X^2- test (with Benjamini-
620 Hochberg correction) was performed for each gene among each of the four
621 subpopulations. Significantly over-represented genes (allowing overlap among
622 subpopulations; $p<0.05$) within subpopulations were also tested.

623 To infer syntenic regions when placing non-orthologous genes of interest back on
624 the *S. viridis* genome, we applied the GENESPACE pipeline[74] to the *S. viridis* genome
625 described herein and five other grasses: *S. italica* (v2.2), *S. bicolor* (v3.1), *O. sativa*
626 ('Kitaake', v3.1), *Z. mays* ('Ensemble-18') and *B. distachyon* (v3.1). Genome
627 annotations and assemblies were downloaded from phytozome
628 (phytozome.jgi.doe.gov). In short, GENESPACE runs the following pipeline. First it
629 parses blast results to the top n (default = 1 * (ploidy / 2)) hits for each gene. A separate

bioRxiv preprint doi: https://doi.org/10.1101/744557; this version posted May 10, 2020. The copyright holder for this preprint (which was not certified by peer review) is the author/funder, who has granted bioRxiv a license to display the preprint in perpetuity. It is made available under aCC-BY-NC-ND 4.0 International license.

orthofinder run is conducted for each pairwise combination of genomes; only blast hits within orthogroups are retained. Syntenic blocks are formed with MCScanX[84] with the block size (-s) and gap (-m) parameters set to 25 and 50 respectively. Blocks are culled to those with high mapping density through 2-dimensional nearest neighbor clustering implemented in the R package dbscan[85]. The resulting pruned collinear blast hits are used as anchors for fixed radius nearest neighbor search based on gene rank. All blast hits within the radius (default r = 100 genes) are considered syntenic. Syntenic blast from all species comparisons are fed into a final orthofinder run and parsed into orthologs and paralogs. Plotting routines are implemented in base R.

Structural Variants

To detect structural variants within the pan-genome, pseudo PacBio reads were generated from assemblies of non-admixed individuals. Pseudo-reads (length: 10kb; depth 5X) were generated from all contigs greater than 10Kb from each pan-genome assembly. The pseudo-reads were aligned to the *S. viridis* reference genome using nglmr (v0.2.7)[86] with default settings for Pacbio reads. The resulting bam file was sorted using samtools (v1.10) and used for calling structural variants with sniffles (v1.0.11). The structural variant types considered across the pan-genome were: insertions, deletions, and inversions. The average number of SV's detected per library was 15,593. A presence/absence matrix for each SV type and was clustered using iterative Kmeans and BIC to determine goodness of fit and the optimal number of clusters present. Based on the BIC criterion, there were three main clusters within the PAV matrix, the first being likely false positives (mean observance 2.8%; n=163,199). The

bioRxiv preprint doi: https://doi.org/10.1101/744557; this version posted May 10, 2020. The copyright holder for this preprint (which was not certified by peer review) is the author/funder, who has granted bioRxiv a license to display the preprint in perpetuity. It is made available under aCC-BY-NC-ND 4.0 International license.

second and third clusters were combined (mean observance 33%; n=33,350) and were used to calculate a distance matrix (method-jaccard) for visualizing subpopulation differences on a PCA plot (Figure 2e).

Population structure

Population structure for both SNP and PAV data was estimated using fastStructure[41] and Admixture[42]. SNP markers were randomly subsetted to 50k by LD pruning (parameters: --indep-pairwise 50 50 0.5) in plink 1.9[87], while shell genes (as determined by DAPC clustering) were extracted from the pan-genome. In both analyses, a single sample with a maximum membership coefficient (qi) of <0.7 was considered admixed. Only non-admixed samples from the SNP analysis were used for further analysis. For SNP markers, multidimensional scaling (MDS), identity by state (IBS), and LD estimates (parameters: --r2 --ld-window-kb 500 --ld-window-r2 0) were performed in plink 1.9.

Extraction of GBS markers from diversity panel assemblies

To integrate previously published GBS data[67] with our new sequencing data, we extracted the relevant GBS markers from the assembled genomes. The paired end sequences were demultiplexed with the sabre package (https://github.com/najoshi/sabre). Samples were aligned to the reference using bwa-mem and SNP were further called using Varscan 2.3.9 (minimum depth of three and variant allele depth of two). SNP with more than 20% missing data in the GBS data were removed, and then those remaining were merged with the diversity panel (598 samples with 8.58M markers). A common set of 55,360 SNP was obtained.

bioRxiv preprint doi: https://doi.org/10.1101/744557; this version posted May 10, 2020. The copyright holder for this preprint (which was not certified by peer review) is the author/funder, who has granted bioRxiv a license to display the preprint in perpetuity. It is made available under aCC-BY-NC-ND 4.0 International license.

676

677 **LD Decay**

678 The extent of LD for the population was determined as described by[88]. For this, first we
679 extracted one SNP every 100bp using plink (--bp-space 100), and selected a random
680 set of 200,000 markers. LD (r^2) was calculated using plink (--ld-window 500 --ld-window-
681 kb 2000). The r^2 value was averaged every 100bp of distance. A nonlinear model was fit
682 for this data in R, and the extent was determined as when the LD (r^2) nonlinear curve
683 reaches 0.2. Average LD was 100 Kbp. This distance defined the window size for
684 searching for candidate genes in the GWAS analyses.

685

686 **Search for *copia* elements**

687 The *copia38* sequence (6.7 kb) was extracted from the genomic sequence of
688 Seita.5G087200 using repbase (https://www.girinst.org/repbase/). Both the *copia38*
689 sequence and *SvLes1* (Sevir.5G085400) sequence (both genomic sequence and CDS)
690 were aligned to each of the pan-genome assemblies (n=598) using blat (-noHead -
691 extendThroughN). From the blat results, each *copia38* alignment was checked whether
692 it fell within the bounds of the *SvLes1* locus.

693

694 **Environmental correlations**

695 Climate data were obtained from WorldClim[52] using the Raster package in R for each of
696 the 577 samples that have geographical coordinates. Correlations were calculated and
697 visualized using the corrplot R package. To account for correlations between the 19
698 bioclimatic variables, we performed Principal component analysis (PCA) using prcomp

bioRxiv preprint doi: https://doi.org/10.1101/744557; this version posted May 10, 2020. The copyright holder for this preprint (which was not certified by peer review) is the author/funder, who has granted bioRxiv a license to display the preprint in perpetuity. It is made available under aCC-BY-NC-ND 4.0 International license.

699 in R. The top three principal components that contribute most of the variance were used
700 independently as response variables in the association analysis. GEMMA[89] was used to
701 identify the association of bioclimatic variables and each of the SNP using only kinship
702 in one model and using both kinship and population structure in another model. For
703 population structure estimation, we first LD-pruned the markers in plink (indep-pairwise
704 50 50 0.5) and selected 50000 random markers. PCA was estimated in plink and the
705 top three components were used as covariates in the mixed model to control for
706 population structure. The best model was evaluated using Quantile-Quantile (Q-Q) plots
707 of the observed vs. expected –log10(p) values which should follow a uniform distribution
708 under the null hypothesis. SNP with p-values less than Bonferroni correction were
709 considered significant. Genes within 100Kbp of a significant marker were also
710 considered significant.
711
712 **Signatures of selection and local adaptation:**
713 We employed two statistics for scanning the genome-wide data for signs of positive
714 natural selection: integrated haplotype score (iHS[90]), and Tajima's D[91]. iHS is based on
715 comparing the extended haplotype homozygosity (EHH) score of the ancestral and
716 derived allele of each marker. This test detects loci where natural selection is driving
717 one haplotype to high frequency, leaving recombination little time to break up the
718 linkage group. This was calculated using hapbin[92]. To find genomic regions associated
719 with natural selection, we estimated the fraction of SNP that have |iHS|>2.0 in each
720 100kbp window, with a slide of 10Kbp. The windows with the highest fraction are
721 considered outliers. Tajima's D[91], compares the average number of pairwise differences

bioRxiv preprint doi: https://doi.org/10.1101/744557; this version posted May 10, 2020. The copyright holder for this preprint (which was not certified by peer review) is the author/funder, who has granted bioRxiv a license to display the preprint in perpetuity. It is made available under aCC-BY-NC-ND 4.0 International license.

722 (π) and the number of segregating sites (S). A negative value indicates positive
723 selection. These values were calculated for 10k windows (with a slide of 10k) and the
724 bottom 1% of the windows were considered outliers.
725
726 **GO and KEGG pathway enrichment analysis**
727 GO enrichment analysis of positively selected genes was performed using topGO[93,94],
728 an R Bioconductor package, to determine overrepresented GO categories across
729 biological process (BP), cellular component (CC) and molecular function (MF) domains.
730 Enrichment of GO terms was tested using Fisher's exact test with $p<0.05$ considered as
731 significant. KEGG[95] pathway enrichment analysis was also performed on those gene
732 sets based on a hypergeometric distribution test and pathways with $p<0.05$ were
733 considered as enriched.
734
735 **GWAS and validation of *SvLes1***
736 The GWAS population to assess seed shattering was planted in the greenhouse
737 facility at Donald Danforth Plant Science Center in April 2014. 215 accessions were
738 chosen from the panel to perform the experiment (Table S8), with four replicates per
739 accession. Shattering phenotype was measured by observing the amount of seed
740 shattering after hand shaking of senesced dry plants. Individual plants were scored
741 using a qualitative scale from 1 to 7. Genotypes were filtered at minor allele frequency >
742 5% for this population. GWAS was performed using a univariate mixed linear model
743 from GEMMA[96], with centered kinship matrix. We used the Wald test p-value[96] for
744 assessing significant peaks, but other p value estimates give similar results. SNP

bioRxiv preprint doi: https://doi.org/10.1101/744557; this version posted May 10, 2020. The copyright holder for this preprint (which was not certified by peer review) is the author/funder, who has granted bioRxiv a license to display the preprint in perpetuity. It is made available under aCC-BY-NC-ND 4.0 International license.

745 effects were identified using snpEff[82]. Deleterious effects of missense SNPs were
746 predicted using PROVEA [53] on both the reference and alternative allele against the
747 NCBI nr protein database.

748 To knockout *SvLes1* we used the backbone pTRANS_250d as described by
749 Cermák et al.[97]. The protospacer of the guide RNAs targeted the first and second exons
750 of *SvLes1*, upstream of the predicted causal mutation to ensure knock out by frameshift
751 (Figure S12a). The binary vector was introduced into callus tissue using AGL1
752 agrobacterium. Tissue culture and transformation followed an established protocol for *S.*
753 *viridis*[98]. T0 and T1 individuals were genotyped to identify newly acquired mutations
754 near the targeted sites. A T2 homozygote *SvLes1-CRISPR1* was obtained and
755 confirmed by Sanger sequencing, together with homozygotes of the unedited reference
756 line for comparison. To test whether the non-shattering phenotype could be attributed to
757 a single gene, we grew out the T3 seed from two presumptive T2 heterozygotes and
758 several presumptive homozygotes and assessed their genotype at *SvLes1* by PCR and
759 sequencing. Three inflorescences per plant were bagged at heading, and the bags left
760 on until about half the seeds in the panicle appeared mature. Seeds that had fallen off in
761 the bag were collected and weighed. Weights fell largely into two categories, either <35
762 mg, or >195 mg, with only a few weights in between, consistent with the effect of single
763 gene.
764

765 **Germination rate, seed weight, and dispersal distance**

766 Seeds from each genotype were collected, incubated at -80˚C overnight, and then
767 chlorine gas sterilized for 4 hours in a bell jar. Glumes were manually removed, and

bioRxiv preprint doi: https://doi.org/10.1101/744557; this version posted May 10, 2020. The copyright holder for this preprint (which was not certified by peer review) is the author/funder, who has granted bioRxiv a license to display the preprint in perpetuity. It is made available under aCC-BY-NC-ND 4.0 International license.

768 seeds were sowed onto 0.5X MS with 1% sucrose plates and incubated in the dark at
769 4˚C for two days. Plates were moved into a growth chamber [12 hours light (156
770 μmol•m^{-2}•sec^{-1}) /12 hours dark, 31˚C days/22 ˚C nights] and percent germination
771 (judged by the emerging radicle tip) was recorded every 24 hours.

772 Seeds were harvested and pooled from five independent plants of each
773 genotype. Five independent replicates of 20 seeds were weighed and recorded.

774 Starting at one week after heading and continuing to maturity, four random plants
775 each from each of two sibling families of *SvLes1-CRISPR1* and wild-type *SvLes1-1*
776 (ME034V) were individually put into a specially designed pot holder in a wind tunnel
777 custom-built for the Kellogg lab with seed collection bins approximately every 10 cm.
778 Blower speed was set to 5 mph for five minutes. Seeds collected in bins at various
779 distances were counted to measure dispersal distance from the parent plant.

780

781 **Tensile strength measurement**

782 Seeds of *SvLes1-1* (ME034v), *SvLes1-2* (A10.1), and *SvLes1-CRISPR1* were
783 treated with 5% liquid smoke overnight at room temperature and kept in wet moss at
784 4°C in the dark for 2-3 weeks. Seeds were sown in Metro mix 360 and grown in a
785 greenhouse with a 14h light/10 h dark cycle, day/night temperatures of 28 and 22°C and
786 relative humidity of 40-50%. Panicles from main stems were collected at 8, 10, 12, 14,
787 16, 18, 20, 24 and 29 days after heading (the apex of the panicles emerged from the
788 leaf sheath). Tensile strength of the spikelet and pedicel junction was measured as
789 described previously[54]. Briefly, panicles were hung upside down from a Mark-10 model
790 M3-2 force gauge. Spikelets were pulled off individually from a panicle using forceps

bioRxiv preprint doi: https://doi.org/10.1101/744557; this version posted May 10, 2020. The copyright holder for this preprint (which was not certified by peer review) is the author/funder, who has granted bioRxiv a license to display the preprint in perpetuity. It is made available under aCC-BY-NC-ND 4.0 International license.

and the peak tension was recorded. Only the most developed spikelets from the central third of the panicle were used to minimize the effects of developmental variation of the spikelets. Six plants with 20 spikelets from each plant were used per genotype per day of measurement. For *SvLes1-1* and *SvLes1-CRISPR1*, the plants in each genotype were offspring of two individual parent plants with the same allele.

Histology

Histological procedures followed [99]. Specifically, primary branches were collected from the central third of panicles 12 and 16 days after heading and fixed in FAA (37% formaldehyde: ethanol: H_2O: acetic acid = 10:50:35:5), followed by a dehydration series in 50%, 70%, 85%, 95%, 100%, 100% and 100% ethanol and 25%, 50%, 75%, 100%, 100% and 100% Histo-Clear (National Diagnostics) series with ethanol as solvent. Paraplast (Leica Biosystems) was then added to each vial of samples and kept overnight, heated at 42°C, and placed in a 60°C oven. The solution was replaced with molten Paraplast twice a day for 3 days. Samples were then embedded in paraffin using a Leica EG1150 tissue embedder, sectioned in 10 μm serial slices with a Leica RM2255 automated microtome, and mounted on microscope slides at 42°C on a Premiere XH-2001 Slide Warmer. Sections were then deparaffinized, rehydrated, stained with 0.05% (w/v) toluidine blue O for 1.5 min, and then rinsed with water, dehydrated in ethanol, cleared with xylene and mounted with Permount Mounting Medium (Electron Microscopy Sciences)[36]. Images were taken using a Leica DM750 LED Biological microscope with ICC50 camera module and Leica Acquire v2.0 software.

bioRxiv preprint doi: https://doi.org/10.1101/744557; this version posted May 10, 2020. The copyright holder for this preprint (which was not certified by peer review) is the author/funder, who has granted bioRxiv a license to display the preprint in perpetuity. It is made available under aCC-BY-NC-ND 4.0 International license.

814 **Domestication selective sweep**

815 Raw sequencing reads of foxtail millet lines were obtained from a previous
816 study[59]. Because the average sequencing coverage in the earlier study (~0.5X) is much
817 lower than in our study, we chose 79 lines (Table S16) that have an estimated coverage
818 > 1X to maximize overlapping SNPs and perform analysis. Briefly, *S. italica* sequences
819 were quality trimmed using sickle[100], and aligned with bwa-mem to our *S. viridis* A10.1
820 genome. Multi-sample SNP calling was performed using samtools and Varscan with a
821 minimum depth of 3. For *S.viridis*, the imputed, phased vcf was used for calculation of
822 π, which uses high coverage. π calculation excluded missing samples. Shared SNPs
823 between foxtail millet and *S. viridis* were combined, and missing data were imputed
824 using Beagle 5.0[101]. Nucleotide diversity values $\pi_{viridis}$ and $\pi_{italica}$ were then calculated
825 using vcftools[102] at 100 kb window size. Using genome-wide nucleotide diversity as a
826 reference, we used the program ms[103] to conduct 100,000 coalescent simulations to
827 estimate the variation range of $\pi_{italica}/\pi_{viridis}$ under a domestication bottleneck model for
828 a window of 20 kb. Strength of the bottleneck was determined by genome wide
829 $\pi_{italica}/\pi_{viridis}$. The estimated ranges were then compared to observed values $\pi_{italica}/\pi_{viridis}$
830 to determine significance of domestication selective sweep regions.

831

832 **Retrotransposon insertion in *S. italica Les1***

833 *Copia38* sequence was obtained from the foxtail millet genomic sequence[104]
834 near the ortholog of *SvLes1*, Seita.5G087200 (Si003873m.g). We confirmed the
835 identity of *Copia38* and identified its LTR region by searching its sequence against
836 repbase (https://www.girinst.org/repbase/). We used blastn[105] to identify close homologs

bioRxiv preprint doi: https://doi.org/10.1101/744557; this version posted May 10, 2020. The copyright holder for this preprint (which was not certified by peer review) is the author/funder, who has granted bioRxiv a license to display the preprint in perpetuity. It is made available under aCC-BY-NC-ND 4.0 International license.

of *Copia38* in the Yugu1[104] and A10.1 genomes. RaxML 8.2.9[106] was used to construct the phylogeny of *Copia38* homologs, and pairwise distances of close homologs to *Copia38* were calculated using Kimura 2 parameter model. Read mapping to Yugu1 genome follows similar procedures described previously. Paired end reads spanning beyond the left and right junction point of *Copia38* were used to determine if the insertion occurs in an accession or not (Figure S12b).

BSA mapping for small leaf angle

The cross between TB159 and A10.1 used pollen of TB159 and follows the protocol described in [107]. F1 individuals were naturally self-pollinated to generate an F2 population. 417 F2 individuals were planted and phenotypically scored, and DNA from 30 small leaf angle individuals was pooled and sequenced. Sequences are available in the SRA at NCBI, BioProject number PRJNA527194 (to be released after publication). The analysis follows the methods described in a previous BSA study in *S. viridis*[40]. Identification of disruptive mutations and missense mutations with deleterious effects follows the same approach described in our GWAS study. Syntenic orthology between *SvLg2* and *liguleless2* in maize was examined and confirmed based on [108].

Acknowledgements

We thank Zhonghui Wang, Xiaoping Li, and Hui Jiang for their help in maintaining the diversity panel and data collection, Dave Kudrna and Rod Wing at Arizona Genomics

bioRxiv preprint doi: https://doi.org/10.1101/744557; this version posted May 10, 2020. The copyright holder for this preprint (which was not certified by peer review) is the author/funder, who has granted bioRxiv a license to display the preprint in perpetuity. It is made available under aCC-BY-NC-ND 4.0 International license.

Institute for high molecular weight DNA extractions, and members of the Miller Lab at the Danforth Plant Science Center for helpful comments on the manuscript.

This work was supported by NSF grants DEB-0115397, MCB-0110809, DEB-0108501, PGRP-0952185, and IOS-1557633 to EAK; and DE-SC0008769 to TPB. The work conducted by the U.S. Department of Energy Joint Genome Institute is supported by the Office of Science of the U.S. Department of Energy under Contract No. DE-AC02-05CH11231.

Author contributions: Credit taxonomy: Conceptualization: IB, TPB, MF, PH, EAK, JS; Methodology: PH, JJenkins, JS; Investigation: CC, KB, MF, AH, PH, JG, JJenkins, JJohnson,TK, JTL, SM, AS, HS, SS, TS, RT, JW, YY; Resources: MF, PH, EAK; Writing - Original Draft: KB, PH, JJ, SM, EAK; Writing - Review & Editing: IB, TPB, MF, PH, EAK, JTL, SM, JS; Visualization: AH, PH, JJ, EAK, JTL; Supervision: IB, TPB, EAK, JS; Project Administration: TPB, EAK, JS; Funding Acquisition: TPB, EAK, JS. Detailed contributions: JS: WGS assembly & sequencing project lead; JJ: map integration, chromosome assembly, analysis; JG: sequencing of BES, QC projects; HS, TK, TS: PacBio sequencing; SS: annotation; MF, PH, EAK: plant collecting; IB, MF, AH, PH, SM: SNP analyses; AH: PAV analyses; JTL: synteny analyses; SM: GWAS of environmental variables; TPB, PH: cloning of *SvLes1*, BSA; PH, EAK, DAN, RT, JW,: phenotyping of *SvLes1*; YY: histology and plant development.

Competing interests: The authors confirm that they have no competing interests.

bioRxiv preprint doi: https://doi.org/10.1101/744557; this version posted May 10, 2020. The copyright holder for this preprint (which was not certified by peer review) is the author/funder, who has granted bioRxiv a license to display the preprint in perpetuity. It is made available under aCC-BY-NC-ND 4.0 International license.

882 **Data availability**: Sequences are available in the SRA at NCBI, BioProject number
883 PRJNA527194 (to be released after publication). Seed stocks for diversity lines are
884 available by contacting co-authors I. Baxter or E. A. Kellogg.
885
886

bioRxiv preprint doi: https://doi.org/10.1101/744557; this version posted May 10, 2020. The copyright holder for this preprint (which was not certified by peer review) is the author/funder, who has granted bioRxiv a license to display the preprint in perpetuity. It is made available under aCC-BY-NC-ND 4.0 International license.

Literature Cited

1 Grass Phylogeny Working Group. Phylogeny and subfamilial classification of the Poaceae. *Annals of the Missouri Botanical Garden* **88**, 373-457 (2001).

2 Kellogg, E. A. *Poaceae*. Pp. 1-416, in K. Kubitzki, ed. *Families and Genera of Vascular Plants* (Springer, 2015).

3 Soreng, R. J. *et al.* A worldwide phylogenetic classification of the Poaceae (Gramineae) II: An update and a comparison of two 2015 classifications. *Journal of Systematics and Evolution* **55**, 259-290, doi:10.1111/jse.12262 (2017).

4 Brutnell, T. P. *et al. Setaria viridis*: a model for C_4 photosynthesis. *Plant Cell* **22**, 2537-2544 (2010).

5 Doust, A. N. & Diao, X.,eds. *The genetics and genomics of Setaria*. Vol. 19 of *Plant Genetics and Genomics: Crops and Models* .(Springer International Publishing, Switzerland, 2017).

6 Doust, A. N., Kellogg, E. A., Devos, K. M. & Bennetzen, J. L. Foxtail millet, a sequence driven grass model system. *Plant Physiology* **149**, 137-141 (2009).

7 Coe, R. A. *et al.* High-throughput chlorophyll fluorescence screening of *Setaria viridis* for mutants with altered CO_2 compensation points. *Functional Plant Biology* **45**, 1017-1025 (2018).

8 Osborn, H. L. *et al.* Effects of reduced carbonic anhydrase activity on CO_2 assimilation rates in *Setaria viridis*: a transgenic analysis. *Journal of Experimental Botany* **68**, 299-310 (2017).

9 Henry, C. *et al.* Sugar sensing responses to low and high light in leaves of the C_4 model grass *Setaria viridis*. *J Exp Bot* **71**, 1039-1052, doi:10.1093/jxb/erz495 (2020).

10 Ermakova, M., Lopez-Calcagno, P. E., Raines, C. A., Furbank, R. T. & von Caemmerer, S. Overexpression of the Rieske FeS protein of the Cytochrome b 6 f complex increases

bioRxiv preprint doi: https://doi.org/10.1101/744557; this version posted May 10, 2020. The copyright holder for this preprint (which was not certified by peer review) is the author/funder, who has granted bioRxiv a license to display the preprint in perpetuity. It is made available under aCC-BY-NC-ND 4.0 International license.

C_4 photosynthesis in *Setaria viridis*. *Commun Biol* **2**, 314, doi:10.1038/s42003-019-0561-9 (2019).

11 Shaw, R. & Cheung, C. Y. M. A mass and charge balanced metabolic model of *Setaria viridis* revealed mechanisms of proton balancing in C_4 plants. *BMC Bioinformatics* **20**, 357, doi:10.1186/s12859-019-2941-z (2019).

12 Saha, P. *et al.* Effects of abiotic stress on physiological plasticity and water use of *Setaria viridis* (L.). *Plant Sci* **251**, 128-138, doi:10.1016/j.plantsci.2016.06.011 (2016).

13 de Souza, W. R. *et al.* Suppression of a single BAHD gene in *Setaria viridis* causes large, stable decreases in cell wall feruloylation and increases biomass digestibility. *New Phytol* **218**, 81-93, doi:10.1111/nph.14970 (2018).

14 Martin, A. P. *et al.* A developing *Setaria viridis* internode: an experimental system for the study of biomass generation in a C_4 model species. *Biotechnol Biofuels* **9**, 45, doi:10.1186/s13068-016-0457-6 (2016).

15 Ferreira, S. S. *et al.* The lignin toolbox of the model grass *Setaria viridis*. *Plant Mol Biol* **101**, 235-255, doi:10.1007/s11103-019-00897-9 (2019).

16 Zhu, C., Yang, J., Box, M. S., Kellogg, E. A. & Eveland, A. L. A dynamic co-expression map of early inflorescence development in *Setaria viridis* provides a resource for gene discovery and comparative genomics. *Front Plant Sci* **9**, 1309, doi:10.3389/fpls.2018.01309 (2018).

17 Yang, J. *et al.* Brassinosteroids modulate meristem fate and differentiation of unique inflorescence morphology in *Setaria viridis*. *Plant Cell* **30**, 48-66, doi:10.1105/tpc.17.00816 (2018).

18 Junqueira, N. E. G. *et al.* Anatomy and ultrastructure of embryonic leaves of the C_4 species *Setaria viridis*. *Ann Bot* **121**, 1163-1172, doi:10.1093/aob/mcx217 (2018).

bioRxiv preprint doi: https://doi.org/10.1101/744557; this version posted May 10, 2020. The copyright holder for this preprint (which was not certified by peer review) is the author/funder, who has granted bioRxiv a license to display the preprint in perpetuity. It is made available under aCC-BY-NC-ND 4.0 International license.

19 Hunter, C. T. *et al. Setaria viridis* as a model for translational genetic studies of jasmonic acid-related insect defenses in *Zea mays*. *Plant Sci* **291**, 110329, doi:10.1016/j.plantsci.2019.110329 (2020).

20 Rodríguez, C. E., Antonielli, L., Mitter, B., Trognitz, F. & Sessitsch, A. Heritability and functional importance of the *Setaria viridis* bacterial seed microbiome. *Phytobiomes* **4**, 40-52 (2020).

21 Agtuca, B. J. *et al.* In-situ metabolomic analysis of *Setaria viridis* roots colonized by beneficial endophytic bacteria. *Mol Plant Microbe Interact* **33**, 272-283, doi:10.1094/MPMI-06-19-0174-R (2020).

22 Ribeiro, A. P. *et al.* Overexpression of BdMATE gene improves aluminum tolerance in *Setaria viridis*. *Frontiers in Plant Science* **8**, doi:10.3389/fpls.2017.00865 (2017).

23 Dangol, A., Yaakov, B., Jander, G., Strickler, S. R. & Tzin, V. Characterizing the serotonin biosynthesis pathway upon aphid infestation in *Setaria viridis* leaves. *bioRxiv* https://doi.org/10.1101/642041 (2019).

24 Liu, Y. *et al.* A biomimetic *Setaria viridis*-inspired electrode with polyaniline nanowire arrays aligned on MoO3@polypyrrole core–shell nanobelts. *Journal of Materials Chemistry A* **6**, 13428-13437, doi:10.1039/C8TA04218G (2018).

25 Yu, Y. & Kellogg, E. A. Inflorescence abscission zones in grasses: diversity and genetic regulation. *Annual Plant Reviews* **1**, 1-35, doi:10.1002/9781119312994.apr0619 (2018).

26 Fuller, D. Q. Contrasting patterns in crop domestication and domestication rates: recent archaeobotanical insights from the Old World. *Annals of Botany* **100**, 903-924 (2007).

27 Harris, D. R. An evolutionary continuum of people-plant interaction, in *Foraging and farming: the evolution of plant exploitation* (eds D. R. Harris & G. C. Hillman) 11-26 (Routledge, 1989).

28 Tanno, K. & Willcox, G. How fast was wild wheat domesticated? *Science* **311**, 1886 (2006).

bioRxiv preprint doi: https://doi.org/10.1101/744557; this version posted May 10, 2020. The copyright holder for this preprint (which was not certified by peer review) is the author/funder, who has granted bioRxiv a license to display the preprint in perpetuity. It is made available under aCC-BY-NC-ND 4.0 International license.

29 Hunt, H. V. *et al.* Millets across Eurasia: chronology and context of early records of the genera *Panicum* and *Setaria* from archaeological sites in the Old World. *Vegetation History and Archaeobotany* **17 (suppl.)**, S5-S18 (2008).

30 Le Thierry d'Ennequin, M., Panaud, O., Toupance, B. & Sarr, A. Assessment of genetic relationships between *Setaria italica* and its wild relative *S. viridis* using AFLP markers. *Theoretical and Applied Genetics* **100**, 1061-1066 (2000).

31 Li, Y. & Wu, S. Traditional maintenance and multiplication of foxtail millet (*Setaria italica* (L.) P. Beauv.) landraces in China. *Euphytica* **87**, 33-38 (1996).

32 Kuta, D. D., Kwon-Ndung, E., Dachi, S., Ukwungwu, M. & Imolehin, E. D. Potential role of biotechnology tools for genetic improvement of “lost crops of Africa”: the case of fonio (*Digitaria exilis* and *Digitaria iburua*). *African Journal of Biotechnology* **2**, 580-585 (2003).

33 Kennard, C., Phillips, L. & Porter, A. Genetic dissection of seed shattering, agronomic, and color traits in American wildrice (*Zizania palustris* var. *interior* L.) with a comparative map. *Theor Appl Genet* **105**, 1075-1086, doi:10.1007/s00122-002-0988-z (2002).

34 Kahler, A. L., Kern, A. J., Porter, R. A. & Phillips, R. L. Maintaining food value of wild rice (*Zizania palustris* L.) using comparative genomics, in *Genomics of Plant Genetic Resources* (eds R. Tuberosa, A. Graner, & E. Frison) 233-248 (Springer Science and Business Media, 2013).

35 Doust, A. N., Mauro-Herrera, M., Francis, A. & Shand, L. Morphological diversity and genetic regulation of seed dispersal in grasses. *American Journal of Botany* **101**, 1759-1769 (2014).

36 Yu, Y., Hu, H., Doust, A. N. & Kellogg, E. A. Divergent gene expression networks underlie morphological diversity of abscission zones in grasses. *New Phytol* **225**, 1799-1815 (2020).

37 Waterhouse, R. M. *et al.* BUSCO applications from quality assessments to gene prediction and phylogenomics. *Mol Biol Evol*, doi:10.1093/molbev/msx319 (2017).

bioRxiv preprint doi: https://doi.org/10.1101/744557; this version posted May 10, 2020. The copyright holder for this preprint (which was not certified by peer review) is the author/funder, who has granted bioRxiv a license to display the preprint in perpetuity. It is made available under aCC-BY-NC-ND 4.0 International license.

988 38 Kellogg, E. A., Aliscioni, S. S., Morrone, O., Pensiero, J. & Zuloaga, F. O. A phylogeny of
989 *Setaria* (Poaceae, Panicoideae, Paniceae) and related genera, based on the chloroplast
990 gene *ndhF*. *International Journal of Plant Sciences* **170**, 117-131 (2009).
991 39 Layton, D. J. & Kellogg, E. A. Morphological, phylogenetic, and ecological diversity of the
992 new model species *Setaria viridis* (Poaceae: Paniceae) and its close relatives. *Amer. J.*
993 *Bot.* **101**, 539-557 (2014).
994 40 Huang, P. *et al. Sparse panicle1* is required for inflorescence development in *Setaria*
995 *viridis* and maize. *Nat Plants* **3**, 17054, doi:10.1038/nplants.2017.54 (2017).
996 41 Raj, A., Stephens, M. & Pritchard, J. K. fastSTRUCTURE: variational inference of
997 population structure in large SNP data sets. *Genetics* **197**, 573-589,
998 doi:10.1534/genetics.114.164350 (2014).
999 42 Alexander, D. H., Novembre, J. & Lange, K. Fast model-based estimation of ancestry in
1000 unrelated individuals. *Genome Res* **19**, 1655-1664, doi:10.1101/gr.094052.109 (2009).
1001 43 Hufford, M. B. *et al.* Comparative population genomics of maize domestication and
1002 improvement. *Nature Genetics* **44**, 808-811 (2012).
1003 44 Shomura, A. *et al.* Deletion in a gene associated with grain size increased yields during
1004 rice domestication. *Nat Genet* **40**, 1023-1028, doi:10.1038/ng.169 (2008).
1005 45 Xu, K. *et al. Sub1A* is an ethylene-response-factor-like gene that confers submergence
1006 tolerance to rice. *Nature* **442**, 705-708, doi:10.1038/nature04920 (2006).
1007 46 Ashikawa, I. *et al.* Two adjacent nucleotide-binding site-leucine-rich repeat class genes
1008 are required to confer Pikm-specific rice blast resistance. *Genetics* **180**, 2267-2276,
1009 doi:10.1534/genetics.108.095034 (2008).
1010 47 Jombart, T. & Ahmed, I. adegenet 1.3-1: new tools for the analysis of genome-wide SNP
1011 data. *Bioinformatics* **27**, 3070-3071, doi:10.1093/bioinformatics/btr521 (2011).

bioRxiv preprint doi: https://doi.org/10.1101/744557; this version posted May 10, 2020. The copyright holder for this preprint (which was not certified by peer review) is the author/funder, who has granted bioRxiv a license to display the preprint in perpetuity. It is made available under aCC-BY-NC-ND 4.0 International license.

48 Jombart, T., Devillard, S. & Balloux, F. Discriminant analysis of principal components: a new method for the analysis of genetically structured populations. *BMC Genet* **11**, 94, doi:10.1186/1471-2156-11-94 (2010).

49 Gordon, S. P. *et al.* Extensive gene content variation in the *Brachypodium distachyon* pan-genome correlates with population structure. *Nat Commun* **8**, 2184, doi:10.1038/s41467-017-02292-8 (2017).

50 Feldman, M. J. *et al.* Components of water use efficiency have unique genetic signatures in the model C_4 grass *Setaria*. *Plant Physiol* **178**, 699-715 (2018).

51 Hellmann, H. & Estelle, M. Plant development: regulation by protein degradation. *Science* **297**, 793-797, doi:10.1126/science.1072831 (2002).

52 Fick, S. E. & Hijmans, R. J. Worldclim 2: New 1-km spatial resolution climate surfaces for global land areas. *International Journal of Climatology* **37**, 4302-4315 (2017).

53 Choi, Y. & Chan, A. P. PROVEAN web server: a tool to predict the functional effect of amino acid substitutions and indels. *Bioinformatics* **31**, 2745-2747, doi:10.1093/bioinformatics/btv195 (2015).

54 Hodge, J. G. & Kellogg, E. A. Abscission zone development in *Setaria viridis* and its domesticated relative, *Setaria italica*. *Am J Bot* **103**, 998-1005, doi:10.3732/ajb.1500499 (2016).

55 Li, C., Zhou, A. & Sang, T. Rice domestication by reducing shattering. *Science* **311**, 1936-1939 (2006).

56 Konishi, S. *et al.* An SNP caused loss of seed shattering during rice domestication. *Science* **312**, 1392-1396 (2006).

57 Zhou, Y. *et al.* Genetic control of seed shattering in rice by the APETALA2 transcription factor *SHATTERING ABORTION1*. *Plant Cell* **24**, 1034-1048 (2012).

58 Lin, Z. *et al.* Parallel domestication of the *Shattering1* genes in cereals. *Nature Genetics* **44**, 720-724 (2012).

bioRxiv preprint doi: https://doi.org/10.1101/744557; this version posted May 10, 2020. The copyright holder for this preprint (which was not certified by peer review) is the author/funder, who has granted bioRxiv a license to display the preprint in perpetuity. It is made available under aCC-BY-NC-ND 4.0 International license.

59 Jia, G. *et al.* A haplotype map of genomic variations and genome-wide association studies of agronomic traits in foxtail millet (*Setaria italica*). *Nat Genet* **45**, 957-961, doi:10.1038/ng.2673 (2013).

60 Odonkor, S. *et al.* QTL mapping combined with comparative analyses identified candidate genes for reduced shattering in *Setaria italica*. *Front Plant Sci* **9**, 918, doi:10.3389/fpls.2018.00918 (2018).

61 Gaut, B. S., Morton, B. R., McCaig, B. C. & Clegg, M. T. Substitution rate comparisons between grasses and palms: synonymous rate differences at the nuclear gene *Adh* parallel rate differences at the plastid gene *rbcL*. *Proc Natl Acad Sci U S A* **93**, 10274-10279 (1996).

62 Pendleton, J. W., Smith, G. E., Winter, S. R. & Johnston, T. J. Field investigations of the relationships of leaf angle in corn (*Zea mays* L.) to grain yield and apparent photosynthesis. *Agron. J.* **60**, 422-424 (1968).

63 Tian, F. *et al.* Genome-wide association study of leaf architecture in the maize nested association mapping population. *Nat Genet* **43**, 159-162, doi:10.1038/ng.746 (2011).

64 Sakamoto, T. *et al.* Erect leaves caused by brassinosteroid deficiency increase biomass production and grain yield in rice. *Nat Biotechnol* **24**, 105-109, doi:10.1038/nbt1173 (2006).

65 Walsh, J., Waters, C. A. & Freeling, M. The maize gene *liguleless2* encodes a basic leucine zipper protein involved in the establishment of the leaf blade-sheath boundary. *Genes Dev* **12**, 208-218, doi:10.1101/gad.12.2.208 (1998).

66 Wang, Z. M., Devos, K. M., Liu, C. J., Wang, R. Q. & Gale, M. D. Construction of RFLP-based maps of foxtail millet, *Setaria italica* (L.) P. Beauv. *Theor. Appl. Genet.* **96**, 31-36 (1998).

67 Huang, P. *et al.* Population genetics of *Setaria viridis*, a new model system. *Molecular Ecology* **23**, 4192-4295 (2014).

bioRxiv preprint doi: https://doi.org/10.1101/744557; this version posted May 10, 2020. The copyright holder for this preprint (which was not certified by peer review) is the author/funder, who has granted bioRxiv a license to display the preprint in perpetuity. It is made available under aCC-BY-NC-ND 4.0 International license.

68 Xiao, C. L. *et al.* MECAT: fast mapping, error correction, and de novo assembly for single-molecule sequencing reads. *Nat Methods* **14**, 1072-1074, doi:10.1038/nmeth.4432 (2017).

69 Chin, C. S. *et al.* Nonhybrid, finished microbial genome assemblies from long-read SMRT sequencing data. *Nat Methods* **10**, 563-569, doi:10.1038/nmeth.2474 (2013).

70 Li, H. Aligning sequence reads, clone sequences and assembly contigs with BWA-MEM. *arXiv* **1303.3997v1 [q-bio.GN]** (2013).

71 McKenna, A. *et al.* The Genome Analysis Toolkit: a MapReduce framework for analyzing next-generation DNA sequencing data. *Genome Res* **20**, 1297-1303, doi:10.1101/gr.107524.110 (2010).

72 Kent, W. J. BLAT--the BLAST-like alignment tool. *Genome Res* **12**, 656-664, doi:10.1101/gr.229202 (2002).

73 Krumsiek, J., Arnold, R. & Rattei, T. Gepard: a rapid and sensitive tool for creating dotplots on genome scale. *Bioinformatics* **23**, 1026-1028, doi:10.1093/bioinformatics/btm039 (2007).

74 Lovell, J. T. *et al.* The genomic landscape of molecular responses to natural drought stress in *Panicum hallii*. *Nat Commun* **9**, 5213, doi:10.1038/s41467-018-07669-x (2018).

75 Haas, B. J. *et al.* Improving the Arabidopsis genome annotation using maximal transcript alignment assemblies. *Nucleic Acids Res* **31**, 5654-5666, doi:10.1093/nar/gkg770 (2003).

76 Smit, A. F. A., Hubley, R. & Green, P. RepeatMasker Open-3.0. (1996-2011).

77 Chapman, J. A. Meraculous2: fast accurate short-read assembly of large polymorphic genomes. *arXiv*, 1608.01031 (2016).

78 Li, H. & Durbin, R. Fast and accurate short read alignment with Burrows-Wheeler transform. *Bioinformatics* **25**, 1754-1760, doi:10.1093/bioinformatics/btp324 (2009).

bioRxiv preprint doi: https://doi.org/10.1101/744557; this version posted May 10, 2020. The copyright holder for this preprint (which was not certified by peer review) is the author/funder, who has granted bioRxiv a license to display the preprint in perpetuity. It is made available under aCC-BY-NC-ND 4.0 International license.

79 Li, H. *et al.* The Sequence alignment/map format and SAMtools. *Bioinformatics* **25**, 2078-2079 (2009).

80 Koboldt, D. C. *et al.* VarScan 2: somatic mutation and copy number alteration discovery in cancer by exome sequencing. *Genome Res* **22**, 568-576, doi:10.1101/gr.129684.111 (2012).

81 Browning, S. R. & Browning, B. L. Rapid and accurate haplotype phasing and missing-data inference for whole-genome association studies by use of localized haplotype clustering. *Am J Hum Genet* **81**, 1084-1097, doi:10.1086/521987 (2007).

82 Cingolani, P. *et al.* A program for annotating and predicting the effects of single nucleotide polymorphisms, SnpEff: SNPs in the genome of *Drosophila melanogaster* strain w1118; iso-2; iso-3. *Fly (Austin)* **6**, 80-92, doi:10.4161/fly.19695 (2012).

83 Sonnhammer, E. L. & Ostlund, G. InParanoid 8: orthology analysis between 273 proteomes, mostly eukaryotic. *Nucleic Acids Res* **43**, D234-239, doi:10.1093/nar/gku1203 (2015).

84 Wang, Y. *et al.* MCScanX: a toolkit for detection and evolutionary analysis of gene synteny and collinearity. *Nucleic Acids Res* **40**, e49, doi:10.1093/nar/gkr1293 (2012).

85 Hahsler, M., Piekenbrock, M. & Doran, D. dbscan: fast density-based clustering with R. *Journal of Statistical Software* **91**, doi: 10.18637/jss.v091.i01 (2019).

86 Sedlazeck, F. J. *et al.* Accurate detection of complex structural variations using single-molecule sequencing. *Nat Methods* **15**, 461-468, doi:10.1038/s41592-018-0001-7 (2018).

87 Chang, C. C. *et al.* Second-generation PLINK: rising to the challenge of larger and richer datasets. *Gigascience* **4**, 7, doi:10.1186/s13742-015-0047-8 (2015).

88 Remington, D. L. *et al.* Structure of linkage disequilibrium and phenotypic associations in the maize genome. *Proc Natl Acad Sci U S A* **98**, 11479-11484, doi:10.1073/pnas.201394398 (2001).

bioRxiv preprint doi: https://doi.org/10.1101/744557; this version posted May 10, 2020. The copyright holder for this preprint (which was not certified by peer review) is the author/funder, who has granted bioRxiv a license to display the preprint in perpetuity. It is made available under aCC-BY-NC-ND 4.0 International license.

89 Zhou, X. & Stephens, M. Efficient multivariate linear mixed model algorithms for genome-wide association studies. *Nat Methods* **11**, 407-409, doi:10.1038/nmeth.2848 (2014).

90 Voight, B. F., Kudaravalli, S., Wen, X. & Pritchard, J. K. A map of recent positive selection in the human genome. *PLoS Biol* **4**, e72, doi:10.1371/journal.pbio.0040072 (2006).

91 Tajima, F. Statistical method for testing the neutral mutation hypothesis by DNA polymorphism. *Genetics* **123**, 585-595 (1989).

92 Maclean, C. A., Chue Hong, N. P. & Prendergast, J. G. hapbin: An efficient program for performing haplotype-based scans for positive selection in large genomic datasets. *Mol Biol Evol* **32**, 3027-3029, doi:10.1093/molbev/msv172 (2015).

93 Alexa, A., Rahnenfuhrer, J. & Lengauer, T. Improved scoring of functional groups from gene expression data by decorrelating GO graph structure. *Bioinformatics* **22**, 1600-1607, doi:10.1093/bioinformatics/btl140 (2006).

94 topGO: Enrichment Analysis for Gene Ontology. R package version 2.24.0 v. 2.24.0 (http://bioconductor.org/packages/release/bioc/html/topGO.html, 2016).

95 Kanehisa, M. & Goto, S. KEGG: Kyoto Encyclopedia of Genes and Genomes. *Nucleic Acids Res* **28**, 27-30, doi:10.1093/nar/28.1.27 (2000).

96 Zhou, X. & Stephens, M. Genome-wide efficient mixed-model analysis for association studies. *Nat Genet* **44**, 821-824, doi:10.1038/ng.2310 (2012).

97 Cermák, T. *et al.* A multipurpose toolkit to enable advanced genome engineering in plants. *Plant Cell* **29**, 1196-1217, doi:10.1105/tpc.16.00922 (2017).

98 VanEck, J., Swartwood, K., Pidgeon, K. & Maxon-Stein, K. *Agrobacterium tumefaciens*-mediated transformation of *Setaria viridis*, in *Genetics and genomics of Setaria Plant Genetics and Genomics: Crops and Models* (eds A. Doust & X. Diao) 343-356 (Springer, 2016).

bioRxiv preprint doi: https://doi.org/10.1101/744557; this version posted May 10, 2020. The copyright holder for this preprint (which was not certified by peer review) is the author/funder, who has granted bioRxiv a license to display the preprint in perpetuity. It is made available under aCC-BY-NC-ND 4.0 International license.

1141 99 Ruzin, S. E. *Plant microtechnique and microscopy*. (Oxford University Press, 1999).

1142 100 A sliding-window, adaptive, quality-based trimming tool for FastQ files (Version 1.33)
1143 Available at https://github.com/najoshi/sickle. (2011).

1144 101 Browning, B. L. & Browning, S. R. Genotype imputation with millions of reference
1145 samples. *Am J Hum Genet* **98**, 116-126, doi:10.1016/j.ajhg.2015.11.020 (2016).

1146 102 Danecek, P. *et al.* The variant call format and VCFtools. *Bioinformatics* **27**, 2156-2158,
1147 doi:10.1093/bioinformatics/btr330 (2011).

1148 103 Hudson, R. R. Generating samples under a Wright-Fisher neutral model of genetic
1149 variation. *Bioinformatics* **18**, 337-338 (2002).

1150 104 Bennetzen, J. L. *et al.* Reference genome sequence of the model plant *Setaria*. *Nature*
1151 *Biotechnology* **30**, 555-561 (2012).

1152 105 Altschul, S. F., Gish, W., Miller, W., Myers, E. W. & Lipman, D. J. Basic local alignment
1153 search tool. *J Mol Biol* **215**, 403-410, doi:10.1016/S0022-2836(05)80360-2 (1990).

1154 106 Stamatakis, A. RAxML version 8: a tool for phylogenetic analysis and post-analysis of
1155 large phylogenies. *Bioinformatics* **30**, 1312-1313, doi:10.1093/bioinformatics/btu033
1156 (2014).

1157 107 Jiang, H., Barbier, H. & Brutnell, T. Methods for performing crosses in *Setaria viridis*, a
1158 new model system for the grasses. *J Vis Exp*, doi:10.3791/50527 (2013).

1159 108 Schnable, J. C., Freeling, M. & Lyons, E. Genome-wide analysis of syntenic gene
1160 deletion in the grasses. *Genome Biology and Evolution* **4**, 265-277 (2012).

1161

bioRxiv preprint doi: https://doi.org/10.1101/744557; this version posted May 10, 2020. The copyright holder for this preprint (which was not certified by peer review) is the author/funder, who has granted bioRxiv a license to display the preprint in perpetuity. It is made available under aCC-BY-NC-ND 4.0 International license.

Figure and Table Legends

Fig. 1. a *Setaria viridis*, in its common highly disturbed habitat next to a road. **b** Average library coverage, contig N50 (Kb), pan-genome assembly size, and number of genes per library; red vertical line in lower right panel represents the number of genes necessary for a library to be included for PAV analysis (n=39,000).

Fig. 2. PAV and SNP diversity of subpopulations. **a** Geographic distribution and population assignment of North American accessions based on SNP data. **b** Geographic distribution and population assignment of Eurasian accessions based on SNP data. **c** PCA of SNP data, showing placement of North American samples among Eurasian ones. **d** PCA of PAV variants, excluding admixed individuals. **e** PCA of structural variants, excluding admixed individuals. Both SNP and PAV data clearly separate the Central-North population (green) from the others, and the structural variants distinguish all populations. *, accession is admixed; black rim on circle, accession is in its native range.

Fig. 3. GWAS and cloning of *Les1*. **a** Manhattan plot of GWAS result, red line showing p=0.01 after Bonferroni correction. **b** Zoom in to peak on Chromosome 5; larger dots represent missense SNPs identified by snpEff. Different colors of missense SNPs indicate Provean score range (blue for >-2.5, green for <-2.5 and >-4.1, red for <-4.1; -2.5 and -4.1 represent 80% and 90% specificity). Lower scores indicate higher likelihood of deleterious effects of the mutation. **c** Table of *Les1* alleles in *S. viridis* (*Sv*)

bioRxiv preprint doi: https://doi.org/10.1101/744557; this version posted May 10, 2020. The copyright holder for this preprint (which was not certified by peer review) is the author/funder, who has granted bioRxiv a license to display the preprint in perpetuity. It is made available under aCC-BY-NC-ND 4.0 International license.

and *S. italica* (*Si*), with structural characteristics, background line, and shattering phenotype. **d** Sanger sequence validating the position of the adenine insertion (frameshift) in *SvLes1-CRISPR-1*.

Fig. 4. Phenotypic characterization of *SvLes1-CRISPR1* mutants and naturally occurring alleles. **a** Force required to break the AZ (tensile strength in gm of force) in *SvLes1-1*, *SvLes1-2*, and *SvLes1-CRISPR1* lines, measured every two days starting at 8 days after heading. **b** Image of *S. viridis* high shattering (*SvLes1-1* in ME034), left two panicles) and *SvLes1-CRISPR1* mutant panicles seven weeks after heading. Both mutants have retained their seed, unlike ME034 which has shed most of its seed at this time point. **c** Seed dispersal distances in a wind tunnel, measured from four independent high shattering plants (*SvLes1-1* in ME034) and eight *SvLes1-CRISPR1* plants at week 6. Wind speed was 5 mph coming from the left of the diagram. The plant, indicated by P, was placed in middle of the tunnel; some seed fell on the windward side (negative distance values) due to oscillation of the plant. Although mean dispersal distance was approximately the same for both alleles, the *SvLes1-CRISPR1* plants released significantly fewer seeds at each distance that the *SvLes1-1* plants.

Fig. 5. Phenotype and mapping of small leaf angle. **a, b** Small leaf angle phenotype in TB159. **c** BSA mapping result, red arrow indicating QTL. **d** Synteny analysis around *SvLg2* and maize *lg2* locus.

Fig. S1. Cumulative citations for *Setaria viridis*, 1960-present, from Scopus, accessed

bioRxiv preprint doi: https://doi.org/10.1101/744557; this version posted May 10, 2020. The copyright holder for this preprint (which was not certified by peer review) is the author/funder, who has granted bioRxiv a license to display the preprint in perpetuity. It is made available under aCC-BY-NC-ND 4.0 International license.

1208 Jan. 2, 2020.

1209

1210 **Fig. S2.** Population distribution and structure of North American accessions.

1211 Population assignment based on SNPs. **a** distribution of all accessions; **b** distribution of

1212 non-admixed samples only; **c** STRUCTURE plot including all accessions.

1213

1214 **Fig. S3.** Over-represented GO categories and KEGG enrichment pathways for each

1215 subpopulation.

1216

1217 **Fig. S4.** Correlations among the bioclim variables[52] for the 577 accessions for which

1218 latitude-longitude information was available.

1219

1220 **Fig. S5.** GWAS results using each of the first three environmental PCs as response

1221 variable. PC1 found no significant loci, PC2 found one, and PC3 found several.

1222

1223 **Fig. S6.** Loci showing significant signatures of selection for each population. Left

1224 column, proportion of SNP with |iHS| >2 for each of the population. Right column,

1225 Tajima's D represented in -ve scale. 100 Kbp windows (slide 10 Kbp). Horizontal lines

1226 represent 95th and 99th percentiles for iHS and 1st and 5th percentiles for Tajima's D.

1227

1228 **Fig. S7. a** Comparison of seed germination rates of *SvLes1-1* and *SvLes1-CRISPR1*

1229 lines. Three plates of Setaria seed with n≥ 53 were measured for germination and

1230 averaged. Error is standard deviation. **b**, Comparison of seed weight of *SvLes1-1* and

bioRxiv preprint doi: https://doi.org/10.1101/744557; this version posted May 10, 2020. The copyright holder for this preprint (which was not certified by peer review) is the author/funder, who has granted bioRxiv a license to display the preprint in perpetuity. It is made available under aCC-BY-NC-ND 4.0 International license.

SvLes1-CRISPR1 lines. Twenty seed weight was measured from 5 independent plants. *SvLes1-CRISPR1* seeds weighed significantly less ($p<0.0001$), but this did not affect germination.

Fig. S8. *SvLes1-2* (A10.1), *SvLes1-1*, and *SvLes1-CRISPR1* have similar anatomical structures in the abscission zone. Spikelets from main panicles 12 days after heading, stained with 0.05% Toluidine blue O. **a,b** *SvLes1-2* (A10.1). **c,d** *SvLes1-1.* **e,f** *SvLes1-CRISPR1.* **a,c,e** Scale bars = 100 µm. **b,d,f** Scale bars **=** 20 µm. En, endosperm; em, embryo. White dotted line, approximate position of AZ.

Fig. S9. Phylogenetic tree of *Copia38* copies in A10.1 and Yugu1 genomes. Red clade shows the recent explosion that contains the copy inserted into *SiLES1*. Gene models in green, *S. italica*; in blue, *S. viridis*.

Fig. S10. Representative dot plots**. a** Dot plot of clone 114809 on a region of scaffold_1. This alignment is representative of the high quality clone alignments in 239 of the 365 available clones. **b** Dot plot of clone 113526 on a region of scaffold_3, which is representative of the 36 clones that landed in repetitive regions of the genome.

Fig. S11. Plots of marker placements for each of the 9 chromosomes (scaffolds) of *S. viridis*.

Fig. S12. **a** guide RNA protospacers and their position relative to allelic mutations and

bioRxiv preprint doi: https://doi.org/10.1101/744557; this version posted May 10, 2020. The copyright holder for this preprint (which was not certified by peer review) is the author/funder, who has granted bioRxiv a license to display the preprint in perpetuity. It is made available under aCC-BY-NC-ND 4.0 International license.

gene model. **b** Method used to detect *Copia38* insertion.

Table S1. Metadata for 598 diversity lines. LIB, library; Q4 max, membership coefficient obtained from the output of STRUCTURE; Q4_subpop, subpopulation assignment using SNP data; Name, collector's name and number or other unique identifier; new name, name in germplasm collection, lat, latitude of original collection; long, longitude of original collection. Subpopulation assignments correspond to those in figures, viz. Magenta -Central - 95 samples; Orange - West coast - 222 samples; Green – Central-North - 148 samples; blue - Central-East - 133 samples. bio1-bio19 are values of environmental variables from the WorldClim database [52]. SRA is the accession number for the Sequence Read Archive at the NCBI.

Table S2. Subpopulation statistics. Numbers of non-admixed individuals based on SNP analysis; numbers used for each subpopulation in the PAV analysis are lower because not all libraries assembled well enough to be used. Number of over-represented genes is the number significant for that subpopulation alone. SNP, single nucleotide polymorphism; Pi/bp, polymorphisms per basepair; IBD, identity by descent for the subpopulation; IBS, identity by state for the subpopulation; LD, linkage disequilibrium; LD R^2>=0.7%, percent of pairwise comparisons with LD>=0.7.

Table S3 PAV diversity by subpopulation, listing over- and under-represented loci.

Table S4. Loadings of bioclim variables on the first three principal components. PC,

bioRxiv preprint doi: https://doi.org/10.1101/744557; this version posted May 10, 2020. The copyright holder for this preprint (which was not certified by peer review) is the author/funder, who has granted bioRxiv a license to display the preprint in perpetuity. It is made available under aCC-BY-NC-ND 4.0 International license.

principal component; min, minimum; max, maximum.

Table S5. Annotation of genes containing markers significantly associated with environmental variables.

Table S6. Significant Biological process GO terms for environmental associations.

Table S7. GO terms and KEGG pathways enriched for loci under selection, as identified by Tajima's D and the absolute value of iHS.

Table S8. *Setaria viridis* samples scored for shattering phenotype. LIB, library number; Name, original accession identified; New_name, internal Brutnell lab identifier; Population, population assignment; Score_lowShatter, shattering index; Allele, nucleotide at position Chr_05:6849363.

Table S9. Comparison of pairwise diversity in the region surrounding *SiLes1* vs. *SvLes1*. Diversity is significantly lower in the *Les1* region in *S. italica* than in *S. viridis*, p=0.0066 based on 100,000 coalescent simulations. Description, interval considered for diversity estimates; total, total number of bp, centered on the gene; either side, number of bp upstream and downstream of the gene.

Table S10. Comparison of linkage disequilibrium (LD) in the region surrounding *SiLes1* vs. *SvLes1*. Intervals as in Table S9.

bioRxiv preprint doi: https://doi.org/10.1101/744557; this version posted May 10, 2020. The copyright holder for this preprint (which was not certified by peer review) is the author/funder, who has granted bioRxiv a license to display the preprint in perpetuity. It is made available under aCC-BY-NC-ND 4.0 International license.

Table S11. Genomic libraries included in the *Setaria viridis* genome assembly and their respective assembled sequence coverage levels in the final release.

*Average read length of PACBIO reads.

Table S12. PACBIO library statistics for the libraries included in the *Setaria viridis* genome assembly and their respective assembled sequence coverage levels.

Table S13. Summary statistics of the initial output of the QUIVER polished MECAT assembly. The table shows total contigs and total assembled base pairs for each set of scaffolds greater than the size listed in the left hand column.

Table S14. Final summary assembly statistics for chromosome scale assembly. Final summary assembly statistics for chromosome scale assembly. Scaffold sequence total is all bases in the release plus gaps. Chromosome sequence is all bases in the chromosomes not including gaps. Total bases is all bases in the release excluding gaps.

Table S15. PAV matrix for all non-admixed individuals.

Table S16. *Setaria italica* lines used for π *italica* - π *viridis* comparison and for test of selective sweeps. Data from [59], downloaded from the Sequence Read Archive at NCBI.